2010-06

Environmental acoustic considerations for passive detection of maritime targets by hydrophones in a deep ocean trench

Biediger, Jeremy S.

Monterey, California. Naval Postgraduate School

NAVAL POSTGRADUATE SCHOOL

MONTEREY, CALIFORNIA

THESIS

ENVIRONMENTAL ACOUSTIC CONSIDERATIONS FOR PASSIVE DETECTION OF MARITIME TARGETS BY HYDROPHONES IN A DEEP OCEAN TRENCH

by

Jeremy S. Biediger

June 2010

Thesis Advisor: Joseph Rice

Approved for public release; distribution unlimited

THIS PAGE INTENTIONALLY LEFT BLANK

REPORT DOCUMENTATION PAGE			Form Approved OMB No. 0704-0188
Public reporting burden for this collection of information is estimated to average 1 hour per response, including the time for reviewing instruction, searching existing data sources, gathering and maintaining the data needed, and completing and reviewing the collection of information. Send comments regarding this burden estimate or any other aspect of this collection of information, including suggestions for reducing this burden, to Washington headquarters Services, Directorate for Information Operations and Reports, 1215 Jefferson Davis Highway, Suite 1204, Arlington, VA 22202-4302, and to the Office of Management and Budget, Paperwork Reduction Project (0704-0188) Washington DC 20503.			
1. AGENCY USE ONLY ***(Leave blank)***	**2. REPORT DATE** June 2010	**3. REPORT TYPE AND DATES COVERED** Master's Thesis	
4. TITLE AND SUBTITLE Environmental Acoustic Considerations for Passive Detection of Maritime Targets by Hydrophones in a Deep Ocean Trench		**5. FUNDING NUMBERS**	
6. AUTHOR(S) Jeremy S. Biediger			
7. PERFORMING ORGANIZATION NAME(S) AND ADDRESS(ES) Naval Postgraduate School Monterey, CA 93943-5000		**8. PERFORMING ORGANIZATION REPORT NUMBER**	
9. SPONSORING /MONITORING AGENCY NAME(S) AND ADDRESS(ES) N/A		**10. SPONSORING/MONITORING AGENCY REPORT NUMBER**	
11. SUPPLEMENTARY NOTES The views expressed in this thesis are those of the author and do not reflect the official policy or position of the Department of Defense or the U.S. Government. IRB Protocol number _____.			
12a. DISTRIBUTION / AVAILABILITY STATEMENT Approved for public release; distribution unlimited		**12b. DISTRIBUTION CODE**	

13. ABSTRACT (maximum 200 words)

This thesis explores the potential advantage of deep ocean trench placement of an acoustic sensor network. The hypothesis is that a hydrophone deployed in a deep ocean trench will operate in an environment of reduced ambient noise such that passive maritime surveillance may be performed with relatively high signal-to-noise ratio (*SNR*). Barrier or "tripwire" coverage along the oceanic trench is made possible by virtue of networked acoustic communication among widely spaced hydrophones. Physics-based hydro-acoustic propagation modeling supports analysis of target-to-sensor propagation and networked acoustic communication links in representative trench environments.

14. SUBJECT TERMS underwater acoustics, Seaweb, Deep Seaweb, undersea noise calculation, ocean trenches, surveillance, anti-submarine warfare, maritime domain awareness, passive detection, reliable acoustic path, sensor network			**15. NUMBER OF PAGES** 81
			16. PRICE CODE
17. SECURITY CLASSIFICATION OF REPORT Unclassified	**18. SECURITY CLASSIFICATION OF THIS PAGE** Unclassified	**19. SECURITY CLASSIFICATION OF ABSTRACT** Unclassified	**20. LIMITATION OF ABSTRACT** UU

NSN 7540-01-280-5500 Standard Form 298 (Rev. 2-89)
Prescribed by ANSI Std. 239-18

THIS PAGE INTENTIONALLY LEFT BLANK

Approved for public release; distribution is unlimited

ENVIRONMENTAL ACOUSTIC CONSIDERATIONS FOR PASSIVE DETECTION OF MARITIME TARGETS BY HYDROPHONES IN A DEEP OCEAN TRENCH

Jeremy S. Biediger
Lieutenant, United States Navy
B.S. Mechanical Engineering, Tulane University, 2001

Submitted in partial fulfillment of the
requirements for the degree of

MASTER OF SCIENCE IN APPLIED PHYSICS

from the

NAVAL POSTGRADUATE SCHOOL
June 2010

Author: Jeremy S. Biediger

Approved by: Joseph A. Rice
Thesis Advisor

Andres Larraza
Chairman, Department of Physics

THIS PAGE INTENTIONALLY LEFT BLANK

ABSTRACT

This thesis explores the potential advantage of deep ocean trench placement of an acoustic sensor network. The hypothesis is that a hydrophone deployed in a deep ocean trench will operate in an environment of reduced ambient noise such that passive maritime surveillance may be performed with relatively high signal-to-noise ratio (*SNR*). Barrier or "tripwire" coverage along the oceanic trench is made possible by virtue of networked acoustic communication among widely spaced hydrophones. Physics-based hydro-acoustic propagation modeling supports analysis of target-to-sensor propagation and networked acoustic communication links in representative trench environments.

THIS PAGE INTENTIONALLY LEFT BLANK

TABLE OF CONTENTS

LIST OF FIGURES

LIST OF ACRONYMS AND ABBREVIATIONS

AOR	Area of Responsibility
ASW	Anti-Submarine Warfare
DI	Directivity Index
DSC	Deep Sound Channel
MDA	Maritime Domain Awareness
NL	Noise Level
RAP	Reliable Acoustic Path
SL	Source Level
SNR	Signal to Noise Ratio
SPSS	Self-Propelled Semi-Submersible
SSP	Sound Speed Profile
TL	Transmission Loss
UUV	Unmanned Underwater Vehicle

THIS PAGE INTENTIONALLY LEFT BLANK

ACKNOWLEDGMENTS

I would like to extend my thanks to my advisor Joe Rice who introduced me to Seaweb and acoustic detection, and guided me in every aspect of my studies and research.

I extend the same gratitude for our technical support from Bill Marn, Bob Creber, and Chris Fletcher at SPAWAR of San Diego. Also, to Gary Wilson at ARLUT for his help on the technical aspects of our sensor equipment and for the assistance during the long but not too difficult days on Key West.

To Gunn, Goh, Bill, Eryn, Paul, and the rest who put up with me these past few years and, in return were supportive and kept all the workdays interesting.

Mostly, I want to say thank you to my loving family; my wife Cynthia for keeping things going when I was not around, and to my beautiful daughters Marisabel and Genevieve. Also thank you to the wonderful staff at CHOMP and Good Samaritan Hospital for helping us out during a difficult time.

THIS PAGE INTENTIONALLY LEFT BLANK

I. INTRODUCTION

Maritime surveillance involves constant vigilance over vast areas of responsibility. Manned platforms, including aircraft, ships, and submarines, are scarce resources requiring costly manpower. They alone cannot meet the requirements for maritime domain awareness.

Unmanned systems are the key to mitigating this shortfall. *In situ* sensors can provide continuous coverage for detecting and classifying maritime vessels of interest. Such a pervasive and persistent sensing capability, coupled with near-real-time communication, would increase the effectiveness of our manned platforms. For cost-effectiveness, the autonomous system can alert on targets when they enter a specific area or choke point. Such an approach allows a sensor network to strategically monitor a larger area with significantly fewer resources for sensing and alerting on targets of interest.

This thesis examines the potential for using naturally occurring deep ocean trenches and ridges as advantageous sites for passive acoustic maritime surveillance.

THIS PAGE INTENTIONALLY LEFT BLANK

II. MARITIME SURVEILLANCE

A. THE NEED FOR MARITIME DOMAIN AWARENESS

The safety and economy of the United States depend upon the security of the world's oceans, thus making maritime domain awareness (MDA) a vital national interest. The continued growth of legitimate international commerce in the maritime domain has been accompanied by a corresponding increase in criminal activity. Conflicts are increasingly characterized by a combination of traditional and irregular tactics, decentralized planning and execution, and non-state actors using both simple and sophisticated technologies in innovative ways [1]. The smuggling of people, drugs, weapons, and other contraband, as well as piracy and terrorism against vessels and ports, pose threats to maritime security [2].

1. Smuggling

Just as the world's oceans are avenues for international commerce, they are also the highways for the movement of illegal commodities. Maritime drug trafficking generates vast amounts of money for international organized crime syndicates and terrorist organizations. In addition to using legitimate commercial shipping, traffickers use special vessels for transportation of contraband such as high-speed watercraft and self-propelled semi-submersibles (SPSS).

2. Piracy and Terrorism

Piracy and incidents of maritime crime tend to be concentrated in areas of heavy commercial maritime activity, especially where there is significant political and economic instability, or in regions with little or no maritime law-enforcement capacity. Today's pirates and criminals are usually well organized and well equipped with advanced communications, weapons, and high-speed craft [2].

Modern terrorists increase their effectiveness and reach by establishing links with sympathetic organizations around the globe. These terrorist groups use shipping as conveyance for positioning their agents, logistical support, and generating revenue [2].

3. Law of the Sea

In 1982, the United Nations set out to define territorial waters and boundaries. The purpose is for controlling and policing of waterways to prevent illegal fishing and dumping. The treaty came about due to an increase in of illegal activities and exploitation of resources in the latter half of the 20th century [3]. Although the United States has not ratified this agreement, other nations are aggressively staking claim to maritime territory.

4. Anti-Submarine Warfare (ASW)

In addition to controlling and preventing criminal activities, MDA involves maintaining military dominance to keep the waterways open and prevent attacks on the homeland [2]. A current ASW thrust is to develop and deploy sensors capable of detecting and classifying modern diesel electric submarines operating in littoral waters or deep ocean environments [4].

5. Environmental Sensing

MDA also involves monitoring the undersea environment for purposes of scientific study including marine mammal tracking, pollution control, oceanography, and detection of seismic events.

6. Interdiction

Effective interdiction of criminal activities and rapid response to other threats are crucial to the MDA strategy. This requires a coordinated effort to share information and resources among military, customs, and law enforcement communities along with the private sector [2]. These actions facilitate more efficient and effective interdiction

operations that are increasingly conducted by long-range, extended-endurance unmanned platforms [5]. Success hinges on the availability of persistent and pervasive sensors, along with near-real-time communication.

B. PREVALENCE OF DEEP OCEAN TRENCHES

Deep ocean trenches exist in every ocean around the globe. They are a result of geologic shifts in the earth's crust or are caused by centuries of erosion [6]. When two tectonic plates collide, the younger of the two plates, because it is less dense, will ride over the edge of the older, heavier plate. The heavier plate plunges steeply through the asthenosphere, forming a trench on the upper crust that can be as much as 75 miles wide, more than a thousand miles long, and several miles deep [6].

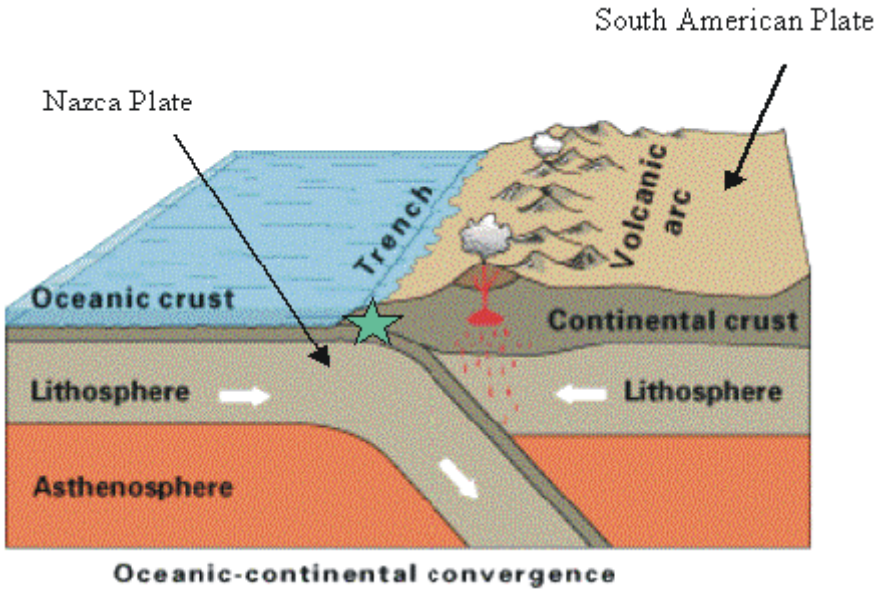

Figure 1. Subduction zone area with related features (from [7]).

The depth of the trench depends on the region and characteristics of the subduction zone fault. The deepest trench, the Marianas, is over 10,000 m at its lowest point while other trenches have depths of 4000 m – 8000 m [8]. Not all oceanic trenches coincide with subduction zone faults. Large height variations between two adjacent plates can result in instabilities and erosion leaving deep crevasses in the bathymetry.

Continental plates tend to be less dense than ocean floors and, as a result, trenches exist along coastal boundaries and are usually much deeper than the adjacent seafloor.

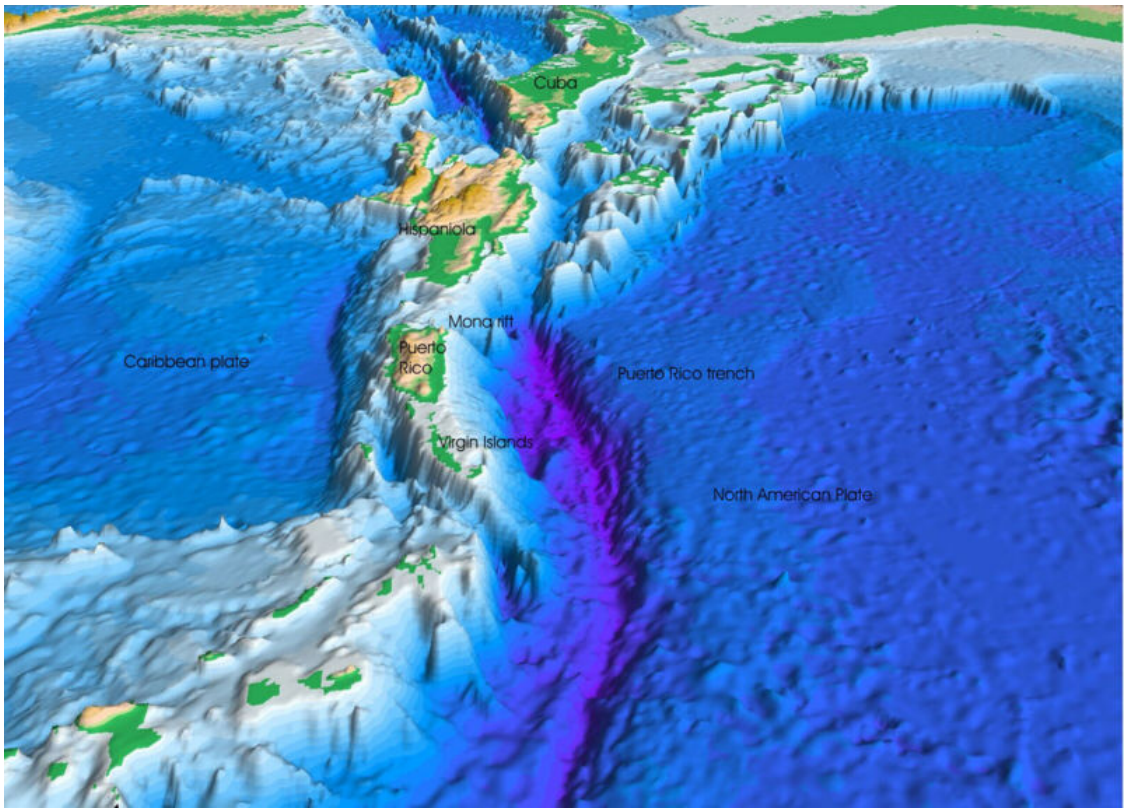

Figure 2. Puerto Rico Trench with perspective view of the Atlantic Ocean and Caribbean Sea floor, which shows the subduction zone cutting along the north shore of Puerto Rico, Hispaniola, and Cuba. The surrounding topography consists of various undersea canyons and islands, including the continental ridge (from [9]).

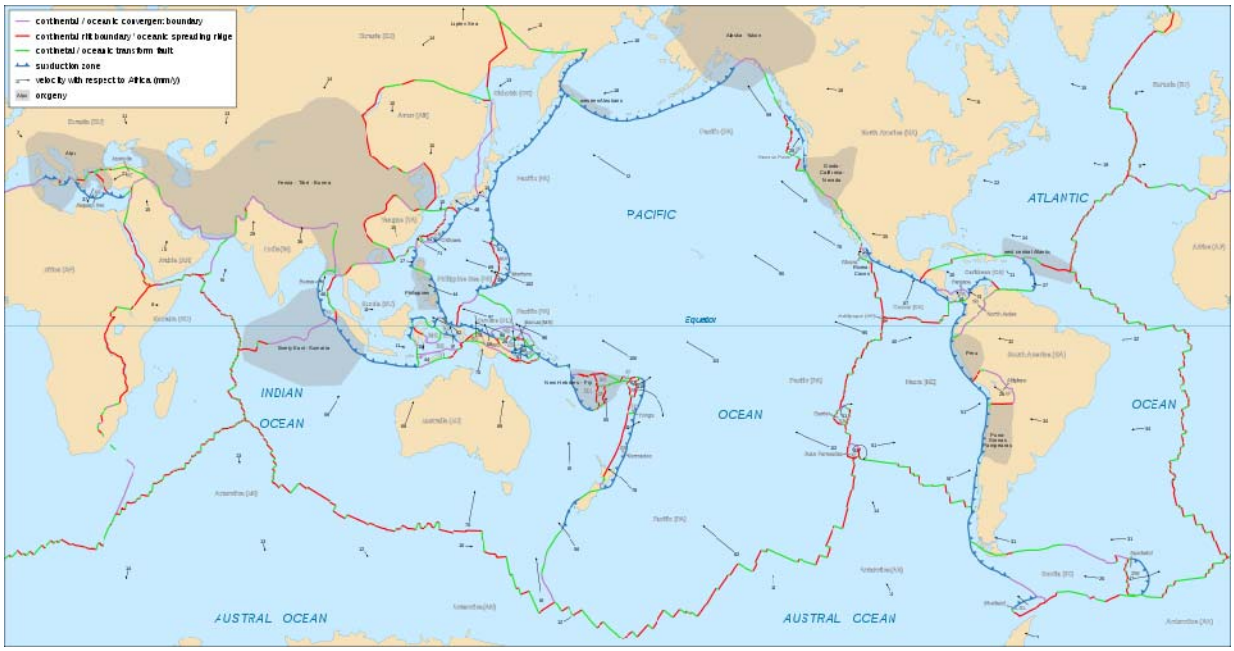

Figure 3. Map showing the geographic location of major fault lines, including the location of subduction trenches (blue lines) (from [10]).

1. Surveillance Tripwire

Traditional maritime surveillance requires assigning a set of assets to an area of responsibility (AOR). Acoustic sensors can monitor the ocean for purposes of detecting and tracking vessels of interest while gathering intelligence on their acoustic signatures and behaviors. This can be effective, even for detecting a target with minimal intelligence prior to interception or if the track of the contact is sporadic. The downside of this approach is that complete vigilance requires populating the entire area with an adequate density of sensors or other assets. Targets will adopt countermeasures to avoid detection or complicate interdiction by law enforcement. Inevitably, the required sensor density must increase with the effectiveness of the countermeasure.

In contrast, a tripwire system does not attempt to provide total coverage for targets of interest but rather will detect their presence at a specific location and alert the response agency. Cueing in this manner efficiently transfers responsibility for interdiction to a capable platform.

A major advantage of this approach is that fewer resources are needed to monitor strategically significant areas with the ability to detect and classify targets of interest. The tripwire approach does have the disadvantage of not providing continuous coverage throughout the AOR. Using an autonomous sensor network as a tripwire requires follow-on prosecution by other platforms and personnel.

2. Trench Exploitation for Improved Detection and Noise Reduction

The proximity of ocean trenches to land makes them suitable sites for early warning tripwires to detect a target of interest moving towards or away from shore. Coastal waters have a logistical advantage in that surveillance can center on areas in which targets will most likely operate. As Figure 4 shows, the required area coverage increases with the radial distance from port. Therefore, placing the system in close proximity to land can help limit the number of sensors required, with the added benefit of ready access for maintenance. Coastal waters also confine movement, due to landmasses that remove essentially half of the area where the vessel may operate, helping to concentrate the search area.

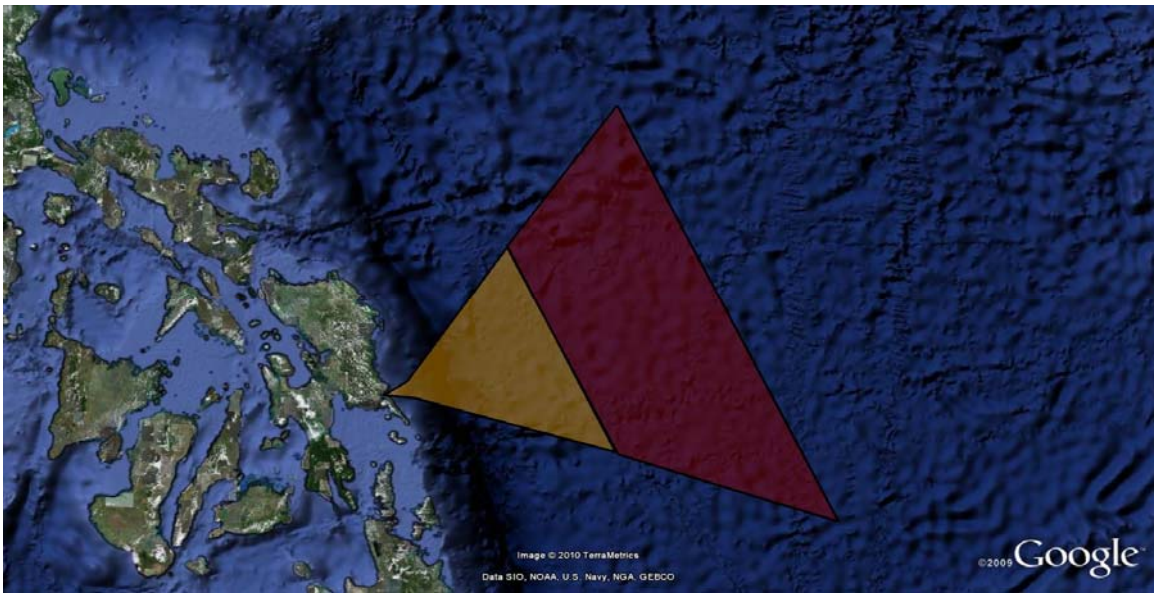

Figure 4. Area of required coverage for adequate surveillance vs. distance from departure point (image and graphic produced using Google Earth).

Placing the sensor network close to land also has disadvantages. The shallower waters along the continental shelf have decreased detection ranges and cannot take advantage of the deep sound channel (DSC). In addition, the high traffic density significantly increases the noise floor and is detrimental to the target *SNR*. Multiple contacts in the search area can also make it difficult to identify a singular vessel. Fishing and dredging in the near-shore waters can also disrupt and damage equipment for the system.

Subduction zone trenches run along certain continental boundaries placing deep ocean environments close to land. The greater depth of the trench can be exploited by a sensor network to gain a large field of view for detecting targets. It is believed that placing sensors at the bottom of a trench will reduce noise arriving from distant sources through blockage by the trench walls surrounding the sensors. This allows utilization of acoustic sensors at areas that are close to land while at the same time minimizing environmental noise and disruption from local traffic.

3. Choke Points

Another method that can work, in conjunction with a deep trench to maximize detection probability, is placing the sensor network at an area of restricted movement. Tracking a target can be facilitated by using geographic features, such as landmasses, which constrain movement and minimize the possible area of operation by the target. Such sites are commonly referred to as choke points.

C. MARITIME SENSOR NETWORKS

1. Seaweb Acoustic Network

Seaweb is an acoustic networking technology for underwater communication among any number of fixed sensor nodes, repeater nodes, and gateway nodes. It is also configurable to communicate with mobile nodes including submarines and unmanned underwater vehicles (UUVs). It enables an autonomous underwater sensor network for

tracking and detecting maritime targets in an area of interest. The challenge in the littorals is to overcome shallow and noisy environments that can limit sensor coverage and communication range [11].

Seaweb's capabilities depend upon several factors in the environment in which it operates. The range of detection is primarily related to the depth of the sensor. Seaweb uses bottom-mounted, upward-looking hydrophones that detect targets in the region of direct-path propagation.

2. Deep Seaweb

Deep Seaweb supports the greater coverage by utilizing the natural advantages of the DSC and the favorable propagation in open ocean areas. A deep trench that runs adjacent to coastal areas provides opportunities for utilizing Deep Seaweb in and around a shallow area to improve coverage and detection as a surveillance tripwire.

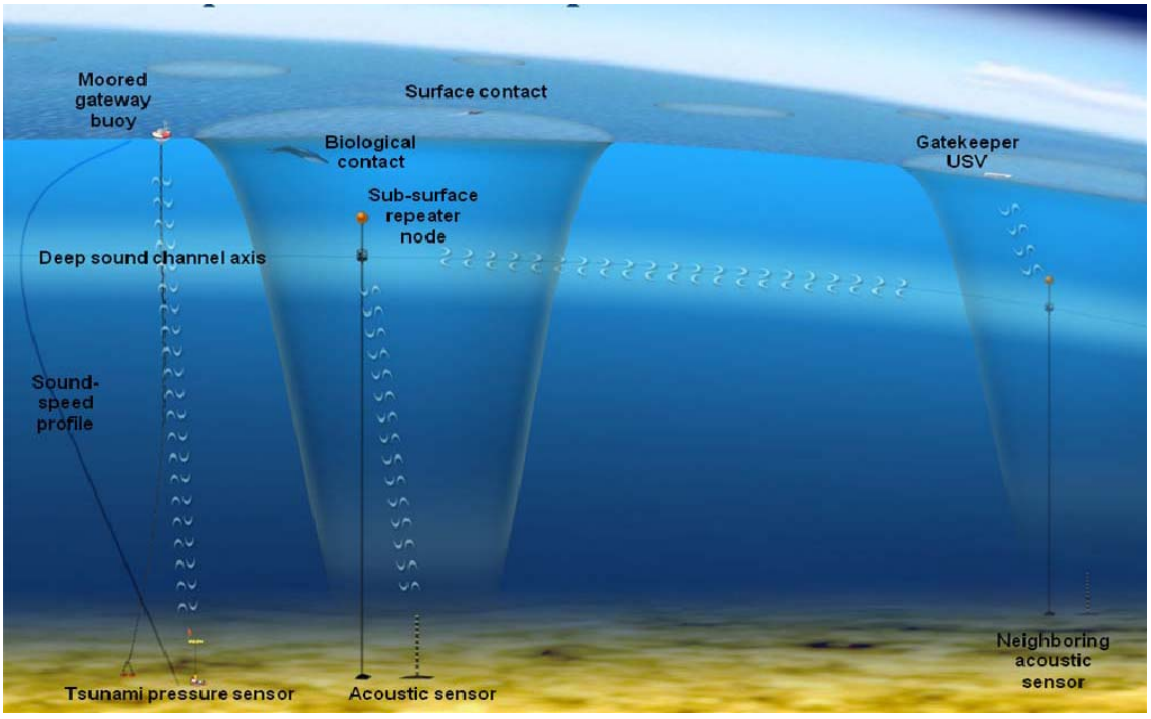

Figure 5. Deep Seaweb Acoustic Network System Concept (from [12]).

III PASSIVE ACOUSTIC SONAR DETECTION

A. SOUND IN THE OCEAN

A variety of sound sources contribute to the ambient noise in the ocean environment. Noise from shipping traffic can travel distances of 1000 miles or more, depending on conditions [13]. The frequency range where this man-made noise is most dominant is from 10 Hz to 300 Hz [13]. Noise level depends on the shipping density surrounding a given area with close proximity to shipping lanes and harbors, implying higher noise levels. Turbulence and flow past the sensor can be a significant factor in ambient noise levels below 100 Hz [13]. A source of very low frequency noise is the earth's seismic activity, which is not significant above 50 Hz [13].

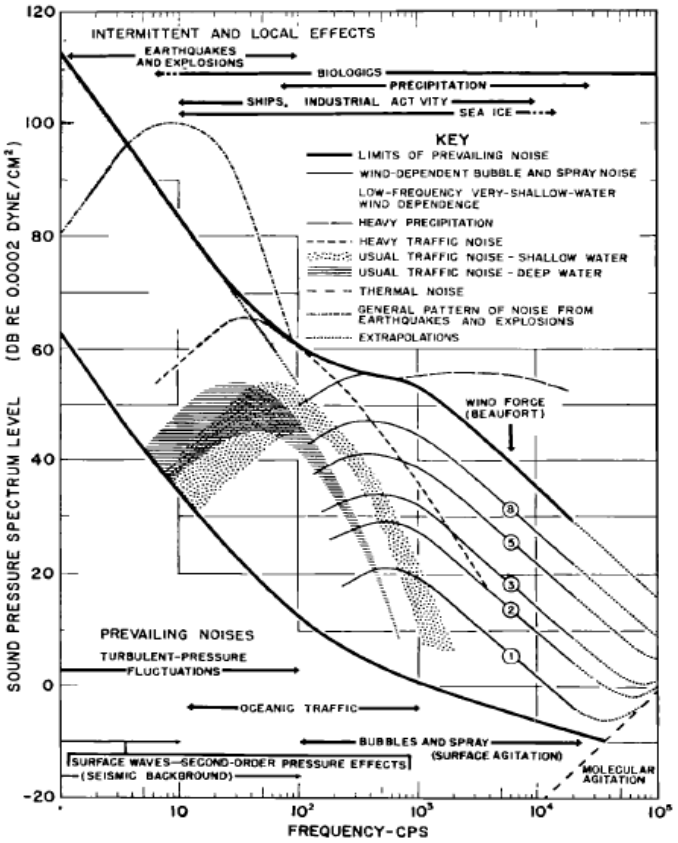

Figure 6. A composite of ambient noise spectra (from [13]).

B. SONAR EQUATION

Each term of the passive sonar equation contributes to the Signal-to-Noise Ratio (*SNR*).

$$SNR = SL - NL - TL + DI \quad (1)$$

Source Level (*SL*) is the energy the source puts in the water. Noise Level (*NL*) is the additional received energy from external activity in the environment as described above. *NL* degrades *SNR* and makes the desired source harder to detect [14].

Transmission Loss (*TL*) is loss suffered through geometric spreading of the source energy and attenuation in the medium. The *TL* depends on water column, water depth, and sea floor characteristics [14].

Directivity Index (*DI*) is the ability of the transducer to physically or electronically direct its received response in space. An omni-directional transducer can detect a signal in all directions and has $DI = 0$. A directional transducer detects better in a certain bearing and has $DI > 0$ dB [14].

For a given sonar system in a given noise environment, if the *SNR* exceeds the detection threshold, the signal can be detected. The use of an acoustic model, such as Bellhop, can identify sensitivities caused by changes in environmental factors [14].

C. ATTENUATION

Signal attenuation in the ocean is caused by numerous effects related to the chemical makeup of seawater. The amount of attenuation experienced is dependent on the frequency of the signal, as seen in Figure 7. Higher frequency energy is attenuated to the surrounding environment or is subject to certain mechanisms such as chemical relaxation and viscosity losses that are not as significant at lower frequencies. Equation 2 is a derivation of the curve from Figure 7 (from [15]).

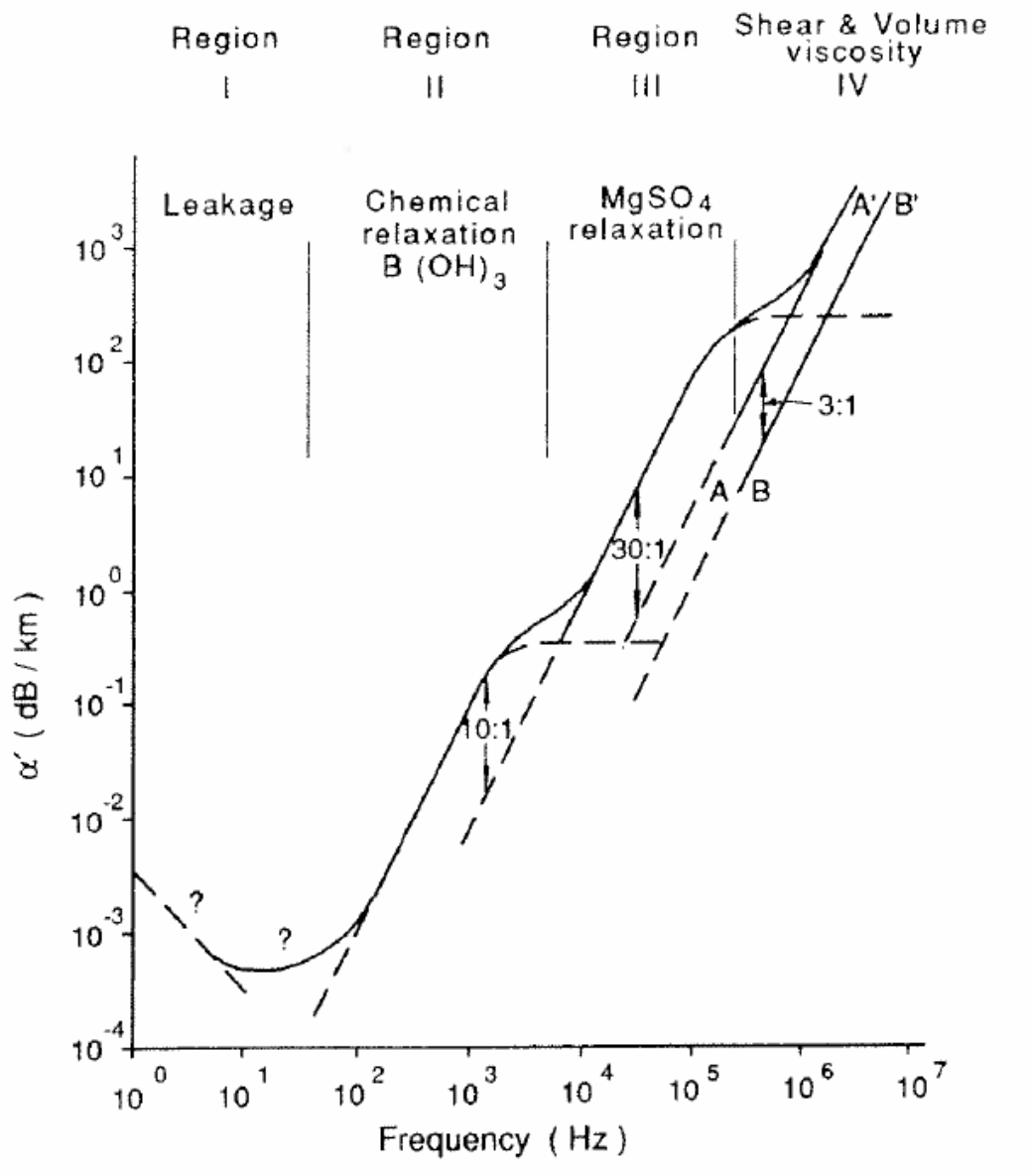

Figure 7. Attenuation vs. Frequency in Seawater (from [15]).

$$\alpha = 3.3\times10^{-3} + \frac{0.11 f^2}{1+f^2} + \frac{44 f^2}{4100+f^2} + 3.0\times10^{-4} f^2 \qquad (2)$$

D. SOUND SPEED PROFILE (SSP)

Sound speed in the ocean varies as a function of temperature, salinity, and pressure. These factors affect sound propagation in the ocean because acoustic waves refract toward slower sound speed areas. Temperature in an area can vary with depth, location, and season, but tends to decrease rapidly with depth in the surface layer before becoming relatively constant. Therefore, sound speed is generally temperature-dependent to around a depth of 1000 m and then is pressure dependent as depth continues to increase. The resultant shape produces a slow-speed propagation duct around 1000 m, known as the DSC. The tendency of sound to want to move toward this duct results in long travel distances without transmission losses from vertical spreading or surface reflection.

Figure 8 shows a representative deep ocean SSP [16] with the DSC at 1000 m depth and the sound speed increasing linearly at depths below the channel. This SSP is assumed in the modeling of acoustic propagation presented in subsequent chapters of this thesis.

The SSP in Figure 8 does not display a mixed layer near the sea surface as would likely be encountered in open ocean environments. In a deep ocean operating environment, where the sensor is bottom-mounted looking upward, the mixed layer will not have significant effect on the sensor performance [14].

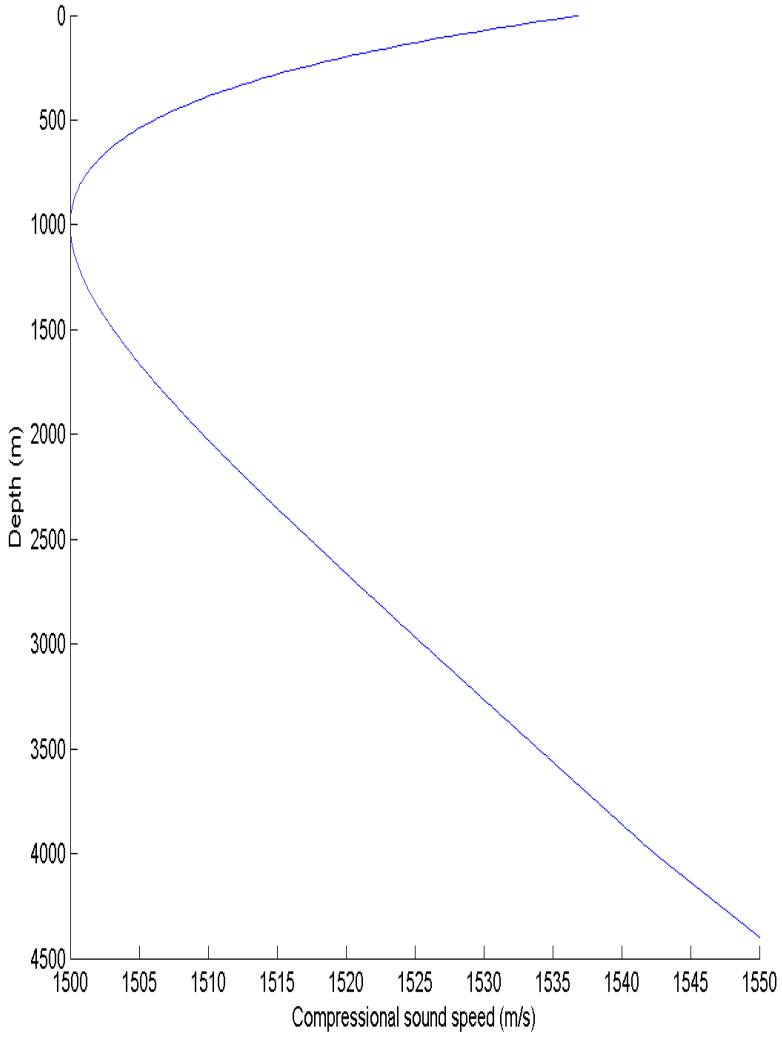

Figure 8. Munk Sound Speed Profile (from [16]).

E. BELLHOP UNDERWATER ACOUSTIC PROPOGATION MODEL

Sound propagation is modeled using the Bellhop ray tracing and beam modeling program, within the AcTUP v2.2l^{α} toolbox, to simulate acoustic transmission from the source to the receivers on the trench bottom and also to demonstrate modem operation within the sound channel [17]. Bellhop is designed to perform two-dimensional acoustic ray tracing and beam forming for a given sound speed field with variable bathymetry and absorption boundaries [18].

THIS PAGE INTENTIONALLY LEFT BLANK

IV. DEEP OCEAN SENSING

This thesis emphasizes sound characteristics at low frequencies where attenuation is less detrimental to the propagation of sound from the target to the sensor. It is also at these frequencies where the presence of machinery tonals and propulsion noise can serve to classify targets of interest. Higher frequency sound is separately considered for purposes of acoustic communications.

A. RECIPROCITY

Modeling of acoustic propagation in this thesis uses the reciprocity rule to more clearly visualize the characteristics of the environment. The sensor is set up as the source in the modeling, with ray data signifying paths the signal travels to the sensor.

B. RELIABLE ACOUSTIC PATH (RAP)

In tropical and temperate deep ocean locales, passive acoustic sensing is most advantageously performed near the ocean floor [14]. Direct-path coverage in deep ocean environments varies with depth and environmental factors, and this coverage area corresponds to the so-called RAP.

1. RAP Range vs. Ocean Depth

In 4000 m water, the direct-path coverage extends to about 28 km from the source, which corresponds to a 7:1 range-to-depth ratio, as observed in Figure 9. In 8000 m water, the range-to-depth ratio decreases to around 5:1 with a range of 40 km, as shown in Figure 10. The SSP has an upward gradient below the DSC axis. As depth below the DSC increases, so does the vertical component of the sound rays, resulting in a greater change in depth for the same horizontal distance traveled.

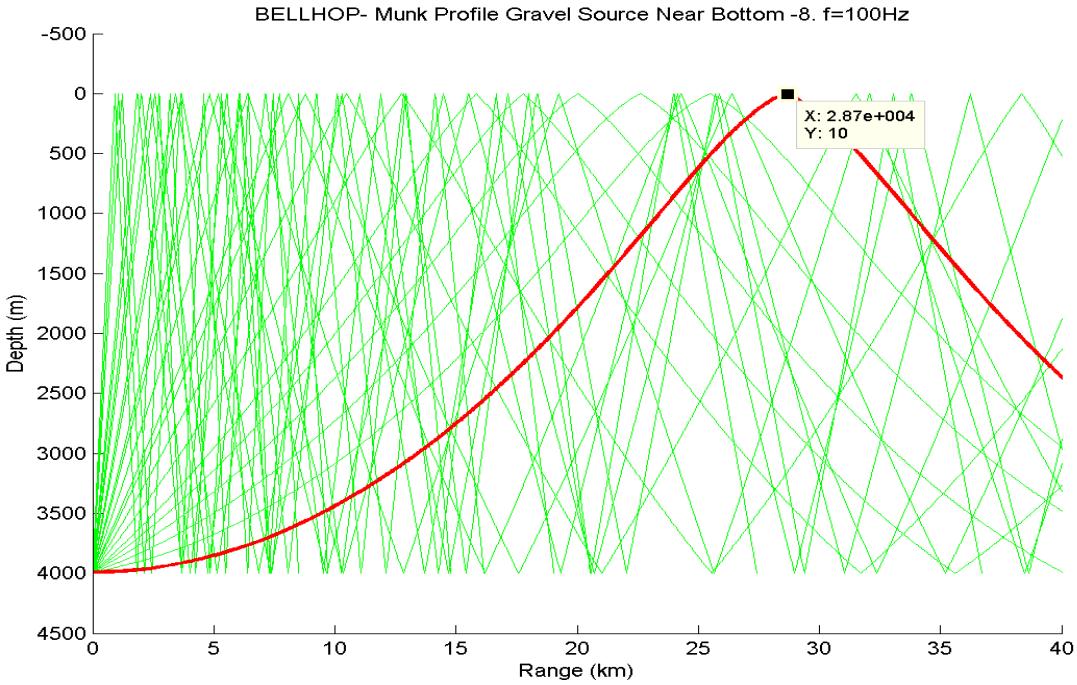

Figure 9. Maximum 100 Hz RAP for 4000 m.

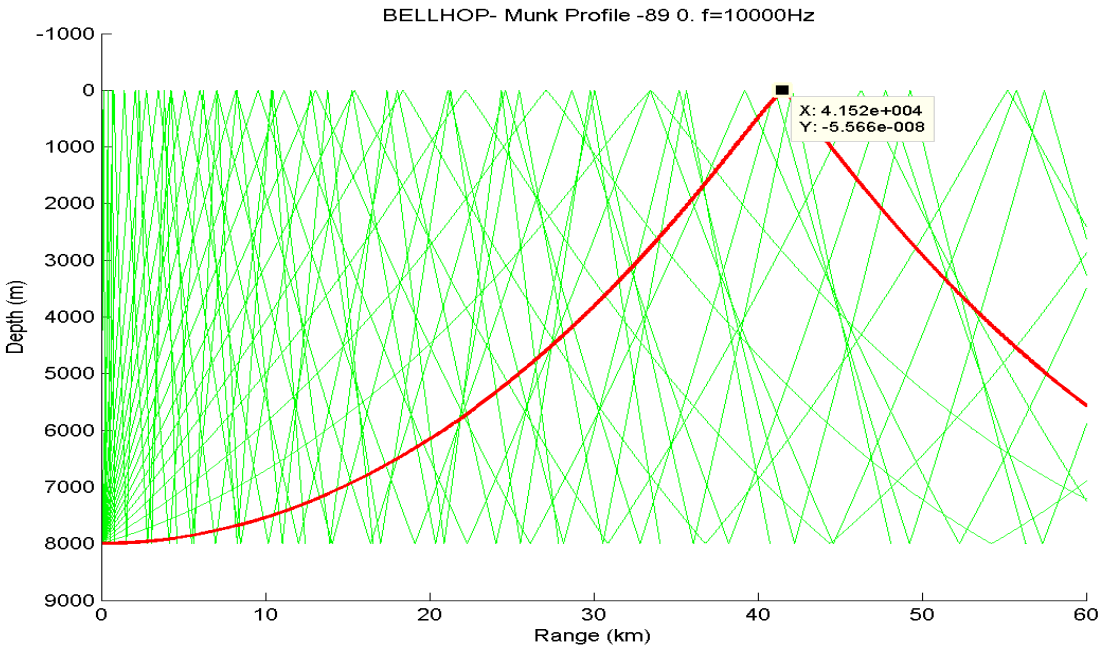

Figure 10. Maximum 100 Hz RAP for 8000 m.

Detection range for the sensor decreases as its depth approaches the DSC until the beam becomes trapped within the channel. At this point the range becomes limited not by direct path but by transmission loss from spreading and attenuation.

2. Transmission Loss Effect on RAP

Figure 11 shows that as range from the sensor increases, so does *TL* even at low frequencies where attenuation is minimal. Spherical spreading significantly reduces *SNR* with an 8 dB loss in the first 12 km of propagation. Depending on the noise level in the area of operation the detection probability will be limited at greater ranges.

In deeper water where the direct-path range is large, spherical spreading again leads to significant transmission loss. However, deep ocean environments tend to have the advantage of lower noise levels that offset this reduced signal.

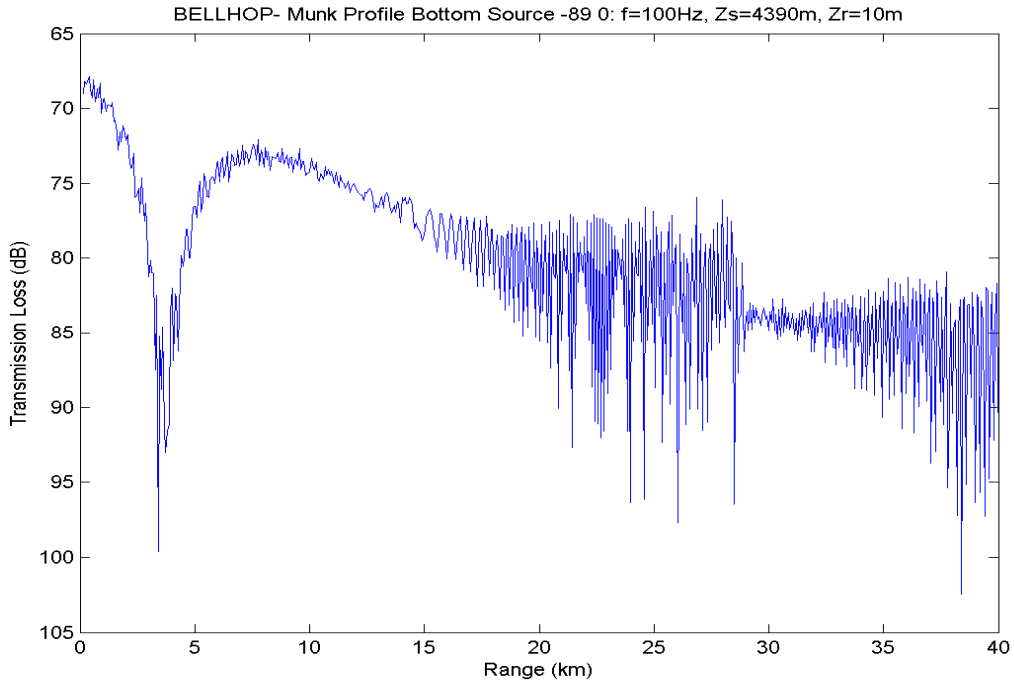

Figure 11. Transmission Loss for 100 Hz; source at 10 m; receiver at 4390 m.

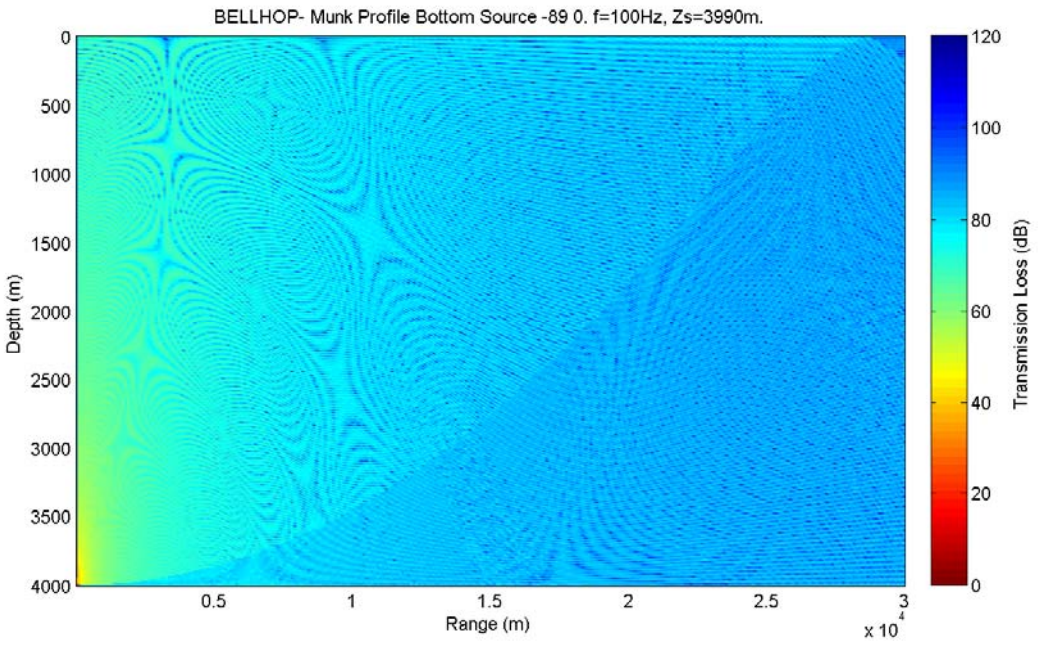

Figure 12. Transmission Loss for 100 Hz; receiver at 3990 m.

C. TRENCH ENVIRONMENTAL FACTORS AND SOUND PROPAGATION

1. Bathymetry

Trenches provide conditions that can be both advantageous and detrimental to acoustic exploitation. The depth provides for greater area coverage and available DSC exploitation near coastal and shallow areas. However, since subduction zone trenches are the result of recent geological and seismic events, the seafloor is uneven and at times unstable. Also, bathymetric features may exist that can hinder operations by blocking or limiting acoustic communications.

2. Sound Modeling for Representative Trench Environments

The shape, size, and geologic makeup of trenches vary significantly depending on location and no singular model can accurately represent the every environment.

Nevertheless, modeling can generally show how bathymetry influences the sound reaching the sensor, which is useful for understanding how the environment may alter surveillance coverage.

For the testing in this thesis, two trench geometries are modeled that correspond to basic bathymetric conditions likely to be encountered in a Seaweb deployment. Trench A is a symmetric canyon that may be an offshoot of a subduction ridge or undersea mountain range. The parameters are 26 km for edge-to-edge, with a depth change of 2330 m and max depth of 4400 m, as shown in Figure 13.

Trench B (Figure 14) is more representative of a subduction zone with a high continental wall (8850 m from edge to bottom) and a lower open ocean wall (3350 m). The cross-sectional width is 113 km from edge to edge.

Both trenches are characterized by reflective rock walls that have a sound speed of c = 1800 m/s. The canonical Munk SSP from Chapter III.D represents the sound speed of the ocean in the trench. Sound speed increases linearly below the DSC corresponding with pressure change as a function of depth.

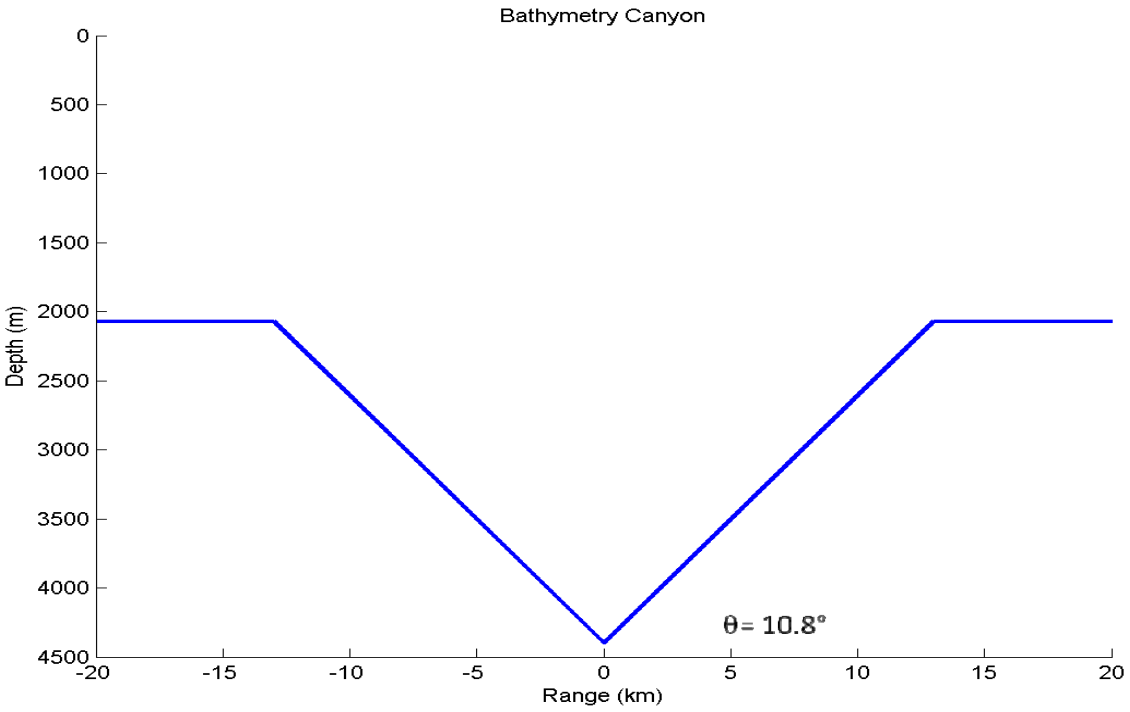

Figure 13. Trench A bathymetry representing a symmetrical canyon.

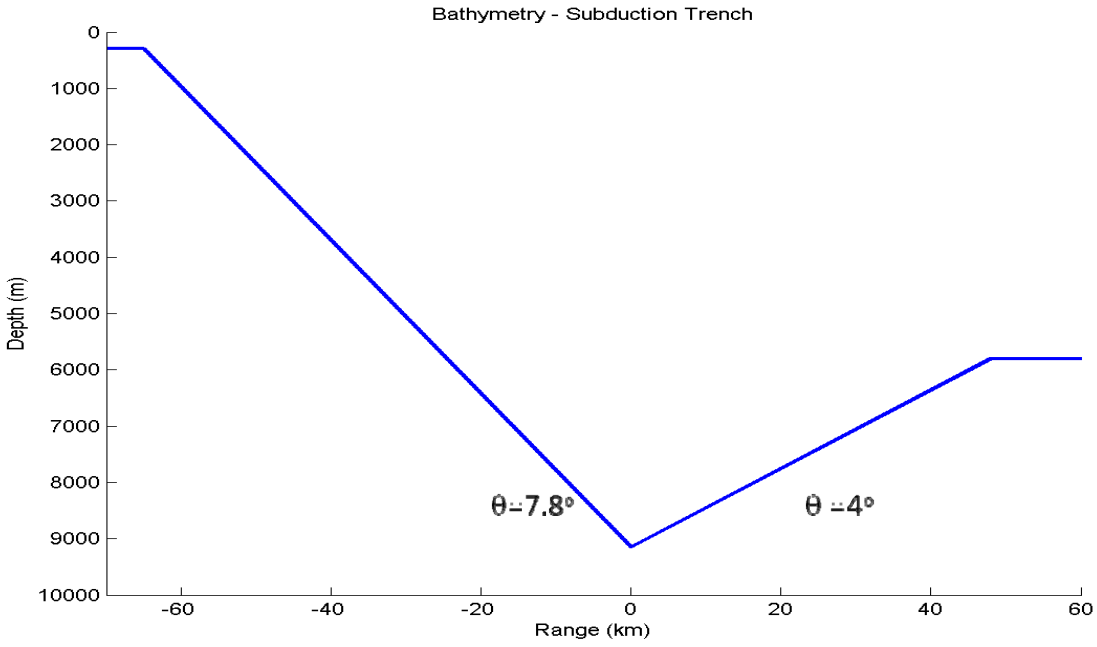

Figure 14. Trench B bathymetry representing a subduction zone.

3. Results for Trench A

The high angled walls of Trench A result in horizontal surveillance range perpendicular to the trench reduced from blockage by the walls. While the detection range is limited by this effect, the walls are also able to concentrate detection in the area that is still visible. Sound that does not reach the sensors directly at lower angles can still reach the sensor by reflection from the angled seafloor. As a result, the sensor may see increased sound energy from the target at certain bearings by a combination of direct and bottom-reflected paths. Figure 15 shows the transmission loss for a flat bottom area while Figure 16 shows how this same area is affected by the trench. Signal drops off outside the trench due to blockage, but areas near the walls see improved signal levels due to the reflective slope. Figure 17 shows that for a target at 10 m below the surface, the trench provides about 5 dB in improved signal energy at 10 km from the sensor.

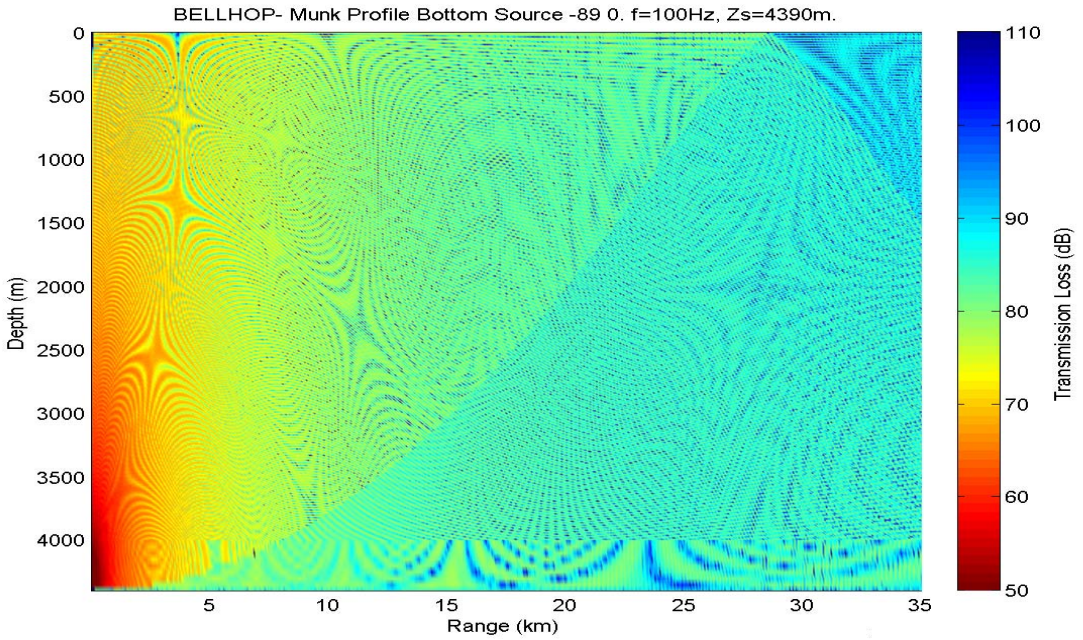

Figure 15. Constant bathymetry 100 Hz Transmission Loss; receiver at 4390 m.

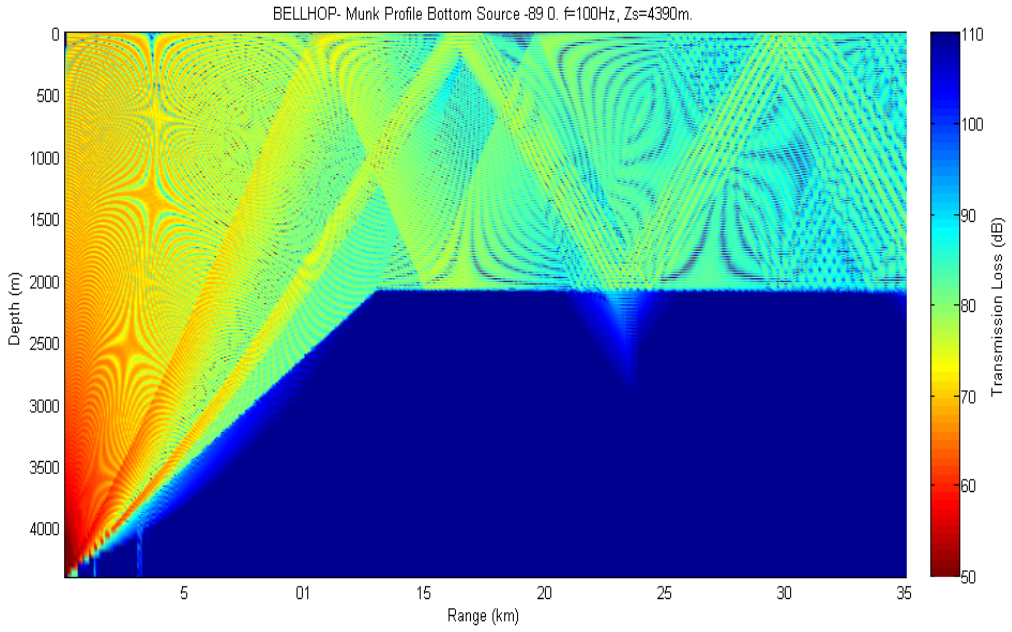

Figure 16. Trench A 100 Hz Transmission Loss; receiver at 4390 m.

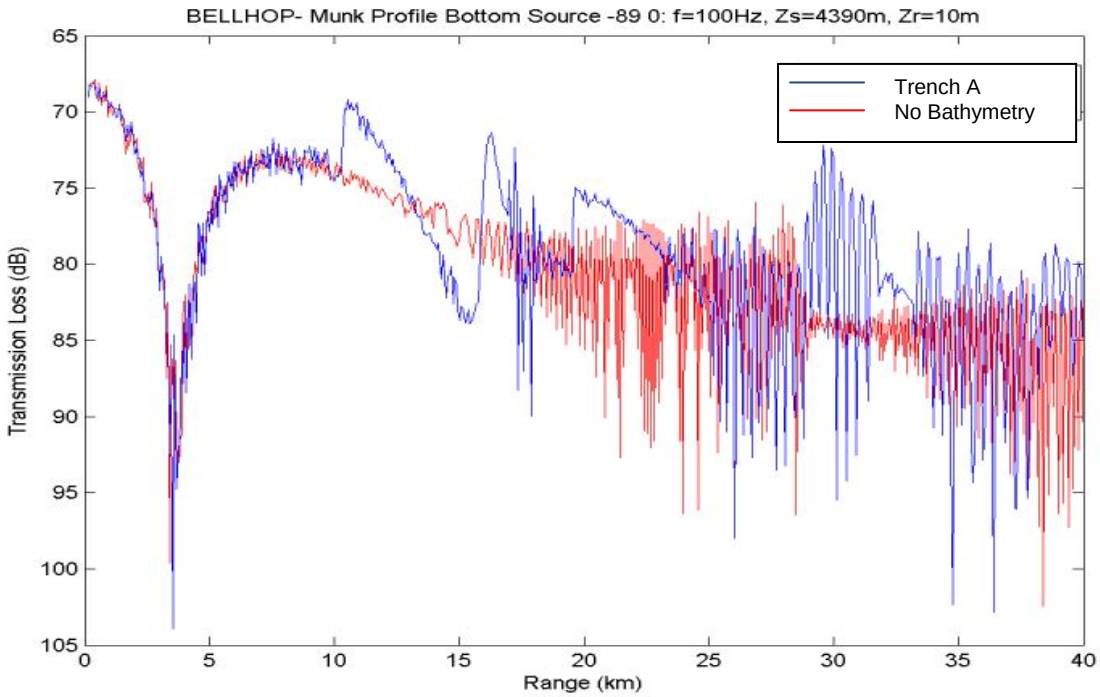

Figure 17. Trench A 100 Hz Transmission Loss; source at 10 m; receiver at 4390 m.

4. Results for Trench B

The lower angle walls present on Trench B provide less focusing of the sound energy than was seen with Trench A. Figure 18 shows that the gain in signal at distant ranges is less significant. With the steeper angle of the high wall, it is expected that its influence would be more significant but, as Figure 19 shows, there is still little effect.

What is of note, in Figure 19, is the dramatic drop in signal level toward the trench edge. A possible explanation is that the shallower depth above the wall, compared with the trench bottom, leaves less room for long-range propagation resulting in more scattering and signal loss before reaching the sensor.

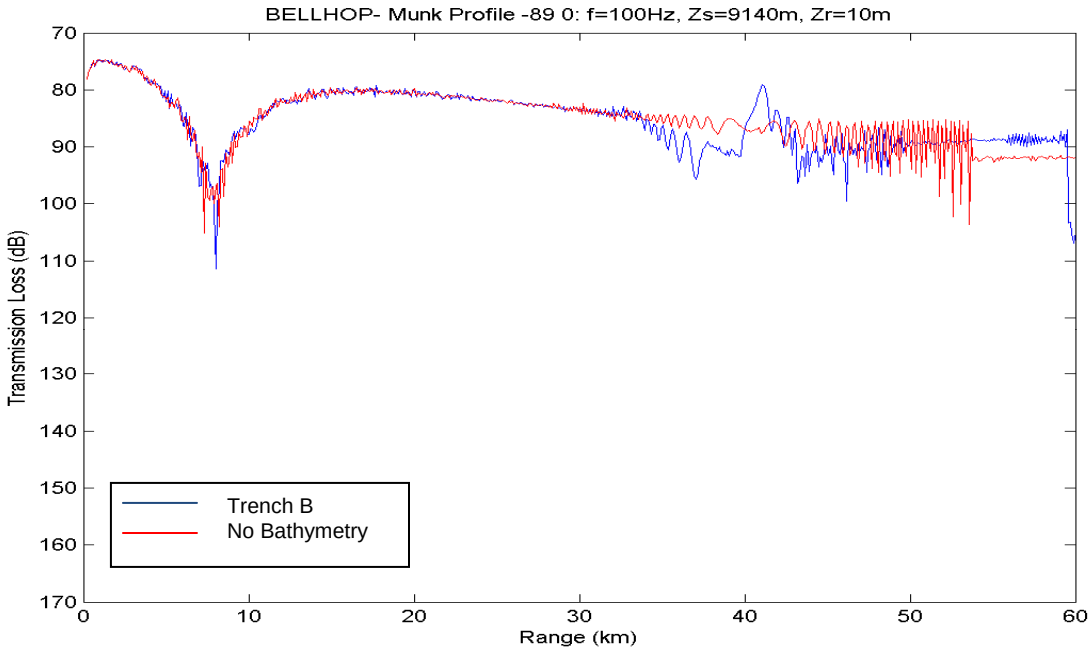

Figure 18. Trench B low wall 100 Hz Transmission Loss; source at 10 m depth; receiver at 9140 m.

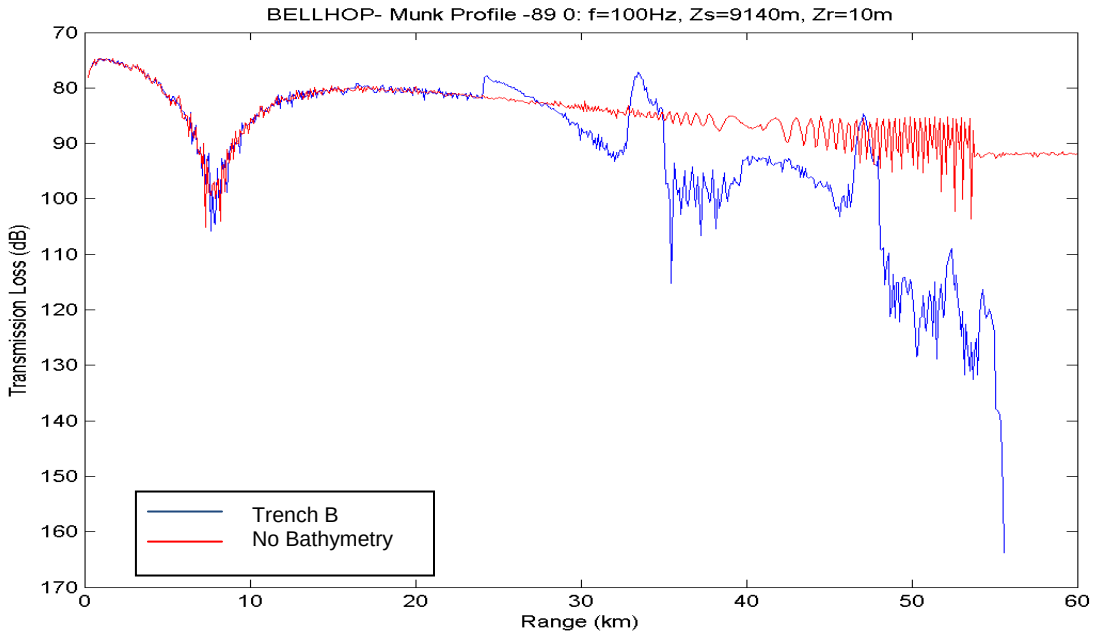

Figure 19. Trench A high wall 100 Hz Transmission Loss; source at 10 m depth; receiver at 9140 m.

5. Examples and Effects of Severe Bathymetry

Trenches A and B represent likely seafloor geometries to be found in many operating environments. In some locations, it may be possible to exploit more extreme geological features to enhance detection. A severe trench with reflective bathymetry will limit the angle of coverage to the shape and angle of the trench walls, but may also greatly focus the cone of detection to a specific area. Trench C, represented in Figure 20, shows an example of a narrow trench shaping the cone of detection. Much energy is lost to reflection, but the trench does provide up to 10 dB of improved signal strength near the vertical axis.

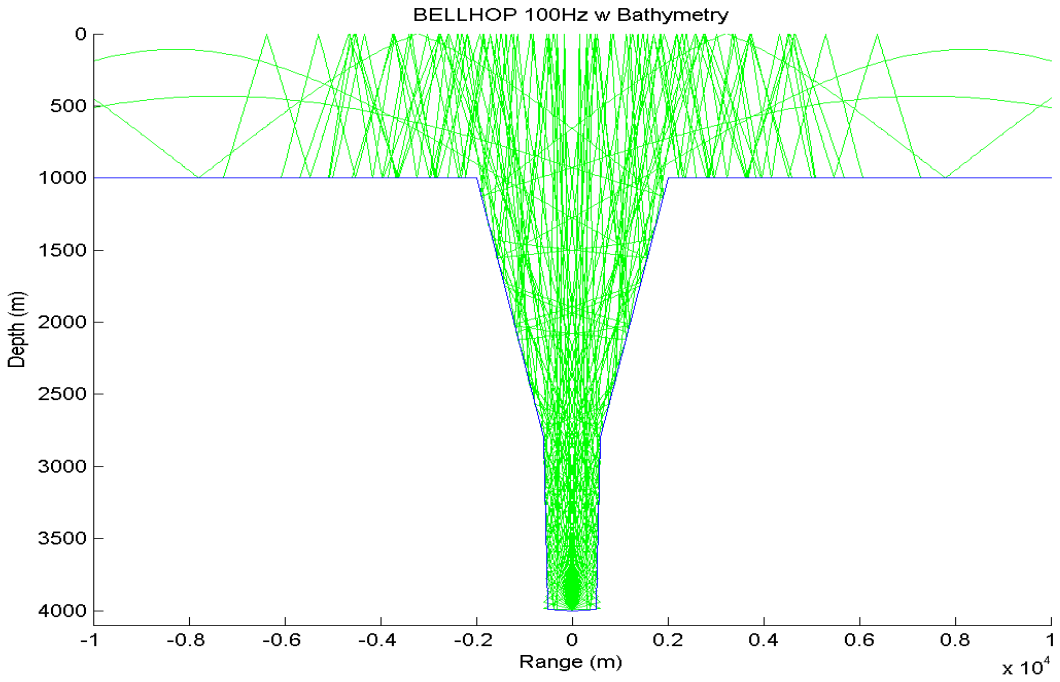

Figure 20. Ray trace diagram Trench C 100 Hz; receiver at 3995 m.

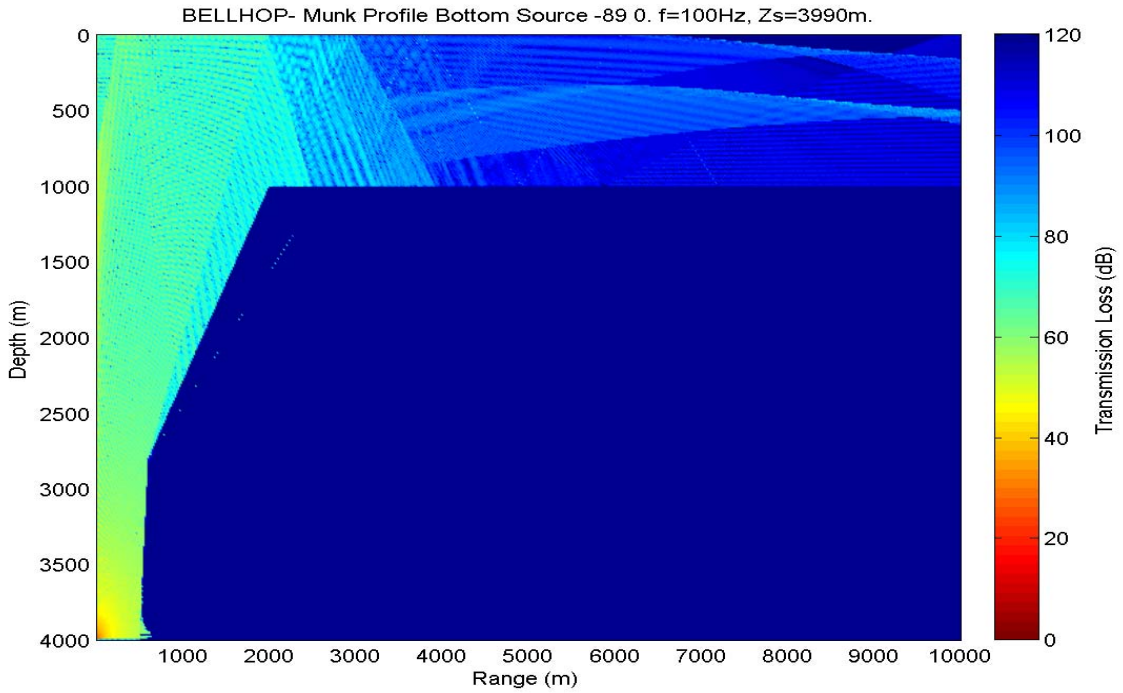

Figure 21. Trench C 100 Hz Transmission Loss; receiver at 3995 m.

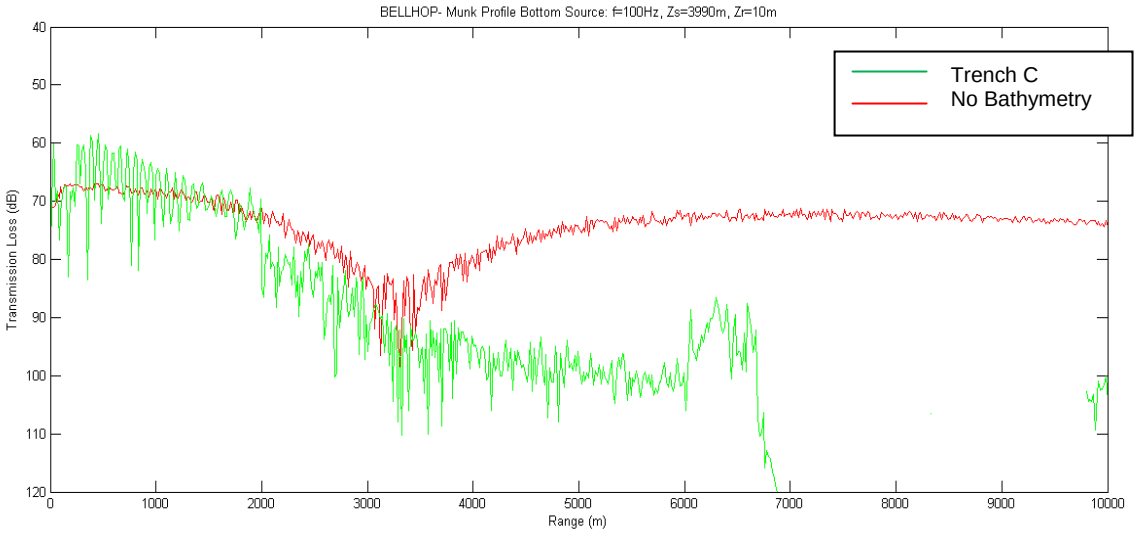

Figure 22. Trench C 100 Hz Transmission Loss; source at 10 m; receiver at 3995 m.

More significant than the increase in signal, is the reduction in ambient noise expected in the trench, which improves *SNR* by decreasing *NL*. Figure 22 shows a large decrease in signal energy outside the trench at 3 km from the receiver. This narrower cone of detection will minimize environmental noise received and will not see contacts that may have previously been visible with a wider cone. This can help in isolating and recognizing a target of interest from other vessels on the water.

While such a narrow trench can provide improved *SNR*, it is an exceptional case that does not account for the more realistic and less ideal conditions expected in an operational environment. A trench usually will not be symmetric in shape, and may likely have a high ridge wall opposite a relatively open ocean environment, as seen in Figure 23.

For modeling Trench D, the simulation combines the cross-sections of a low trench (Figure 24) with the steep wall of the Trench C (Figure 20). The high wall acts similar to the narrow trench by deflecting noise above the sensor, leading to reduced *TL* and *NL*. Figure 25 shows improved signal strength above the sensor and at 8500 m. The lack of a wall opposite the high ridge prevents reflection towards the ridge side. The result of this is a blind spot above the wall. Figure 26 shows that detection rapidly decreases at ranges greater than 2 km from the sensor. This can be beneficial in contact separation if the wall is blocking a shipping lane or high-traffic area that can otherwise mask target detection.

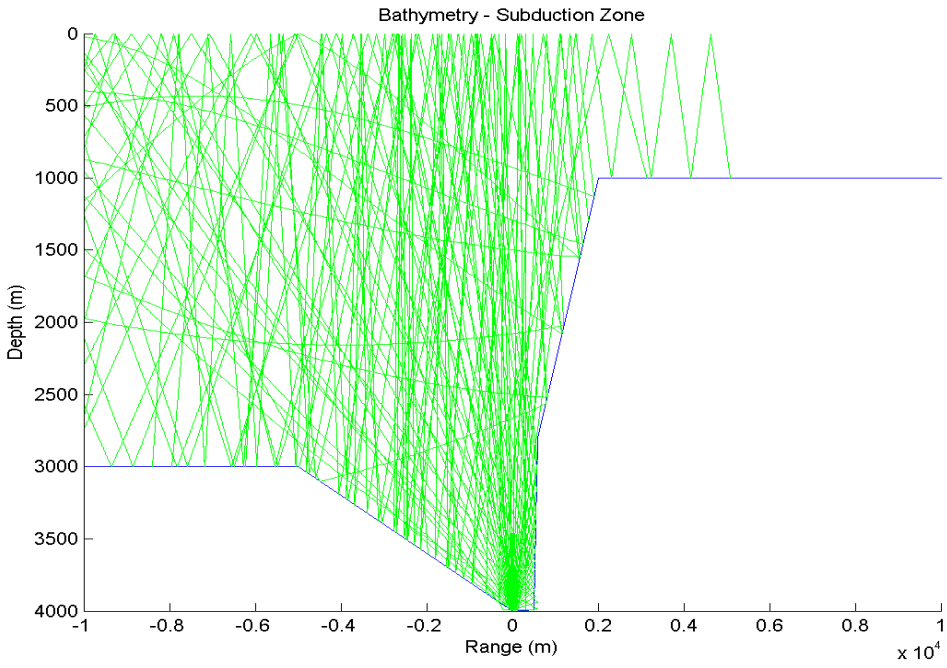

Figure 23. Ray trace diagram Trench D; receiver at 3995 m.

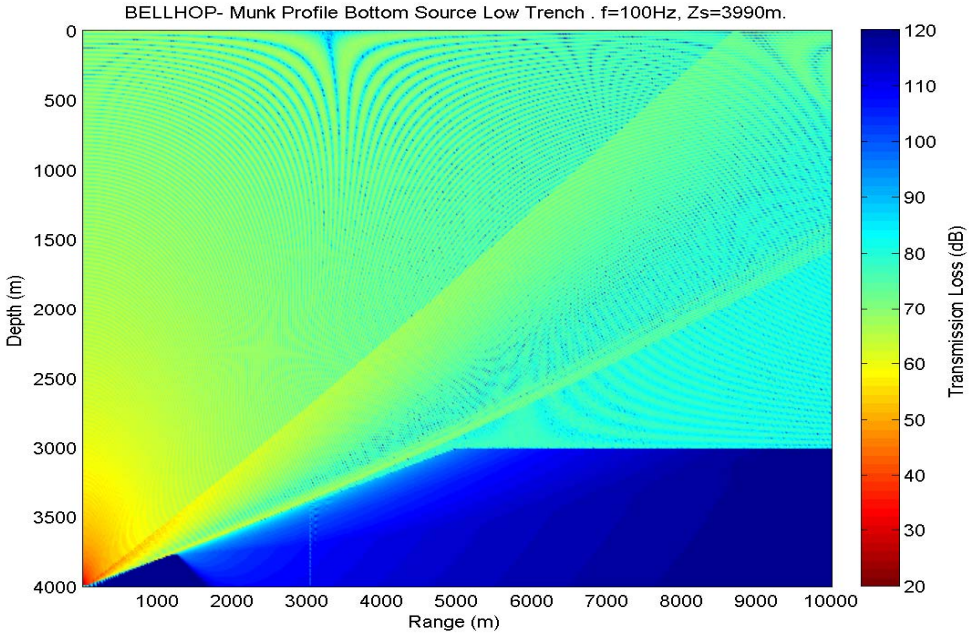

Figure 24. Trench D low wall 100 Hz Transmission Loss; receiver at 3995 m.

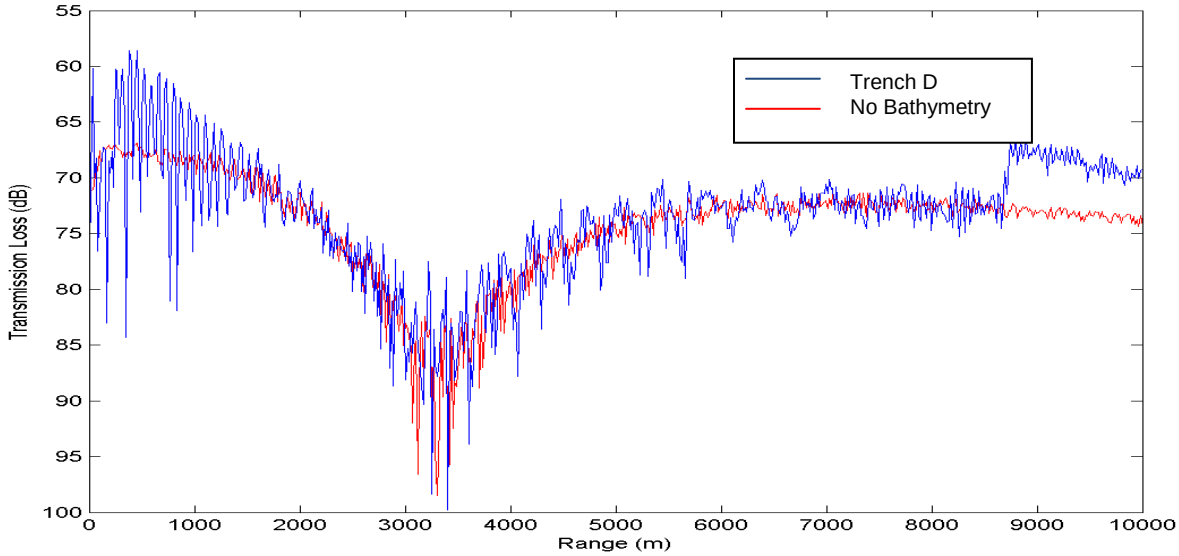

Figure 25. Trench D low wall 100 Hz Transmission Loss; source at 10 m depth; receiver at 3995 m.

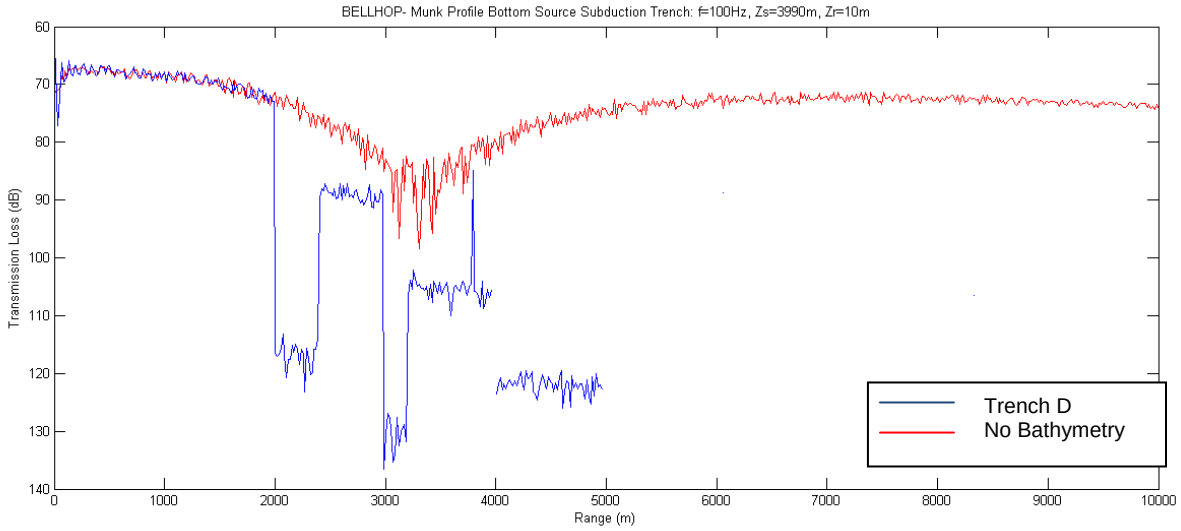

Figure 26. Trench D high wall 100 Hz Transmission Loss; source at 10 m depth; receiver at 3995 m.

THIS PAGE INTENTIONALLY LEFT BLANK

V. NOISE EFFECT ON DETECTION

A. NOISE DIRECTIONALITY IN THE DEEP OCEAN

At low frequencies, noise arrives at a bottom-mounted deep ocean sensor predominantly from the horizontal direction rather than from overhead, while the opposite is true at high frequencies. Figure 27 shows the decibel change in ambient noise *NL* as a result of vertical beam angle (θ) at the receiver.

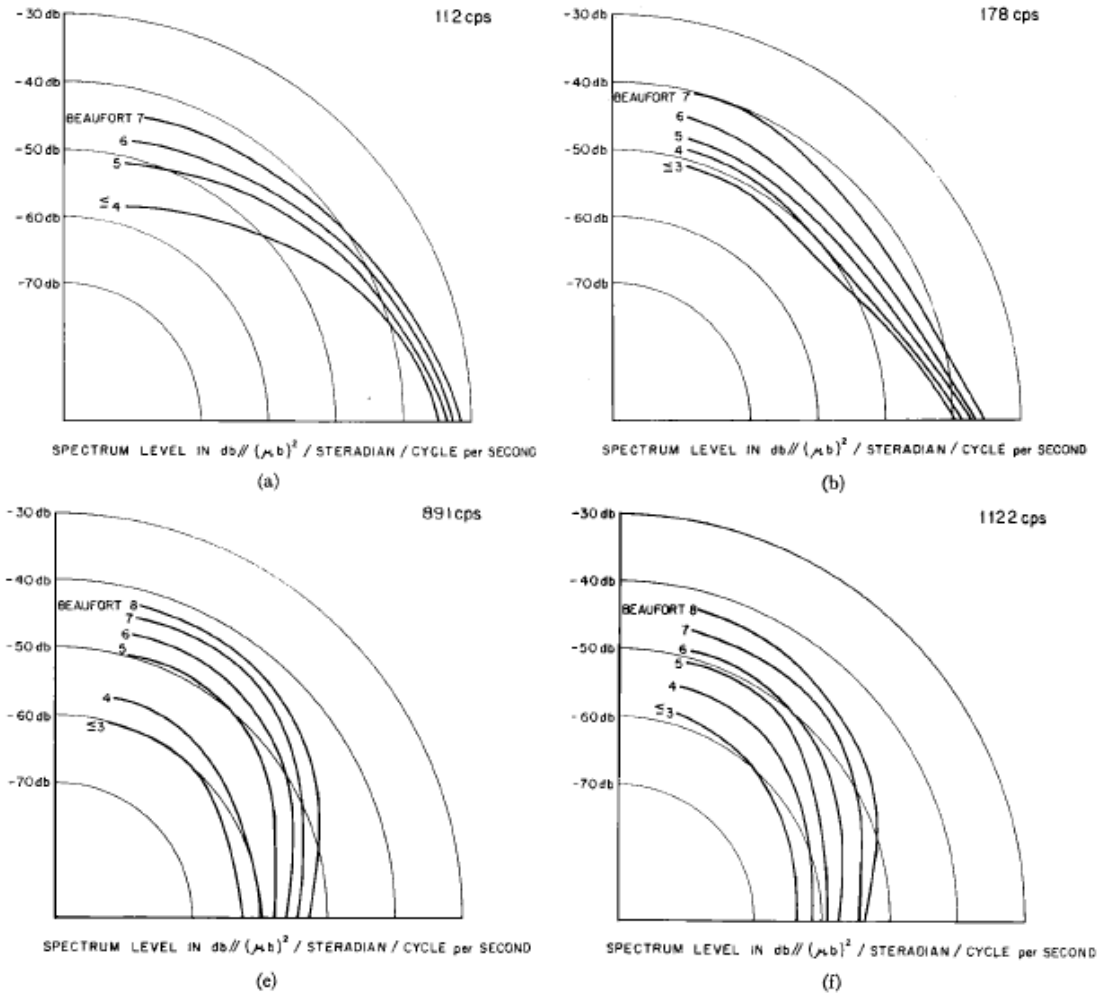

Figure 27. Noise Directionality polar plot with Beaufort number (from [19]).

Noise emanating from distant sources arrives at the receiver near the horizontal with the high frequency components strongly attenuated in transit. Noise from the vertical originates from sources above the sensor and is subject to much less attenuation by virtue of the shorter distance. Higher frequency noise energy arriving at near vertical angles apparently originates near the sea surface and is strongly dependent on wind conditions, as measured on the Beaufort scale [19].

B. NOISE CHARACTERISTICS IN A TRENCH ENVIRONMENT

Since propagation of lower frequency sound is sustained at great distances in the ocean, noise energy below 300 Hz is a large component of the noise received at the sensor. Figure 6 shows that most tonals and shipping noise are at low frequencies. Therefore, low-frequency ambient noise can adversely affect *SNR*. Canyon walls and other bathymetric features can act to both emphasize a signal from overhead and, at the same time, suppress noise from distant sources.

C. CALCULATING NOISE LEVELS AT A SENSOR

Noise spectrum level at the bottom-mounted hydrophone for a given look azimuth ϕ is formulated as:

$$N_{\phi} = \int_{\theta_o(\phi)}^{\frac{\pi}{2}} N(\theta) d\theta \tag{3}$$

where θ is the vertical look angle, $\theta = \theta_o(\phi)$ is the elevation slope of the trench wall in the look azimuth ϕ, and $\theta = \pi/2$ is the vertical upward looking direction.

The curve in Figure 28 is converted to linear intensity from decibels (dB), using Equation 4.

$$N_I(\theta) = 10^{\frac{N_{dB}(\theta)}{10}} \tag{4}$$

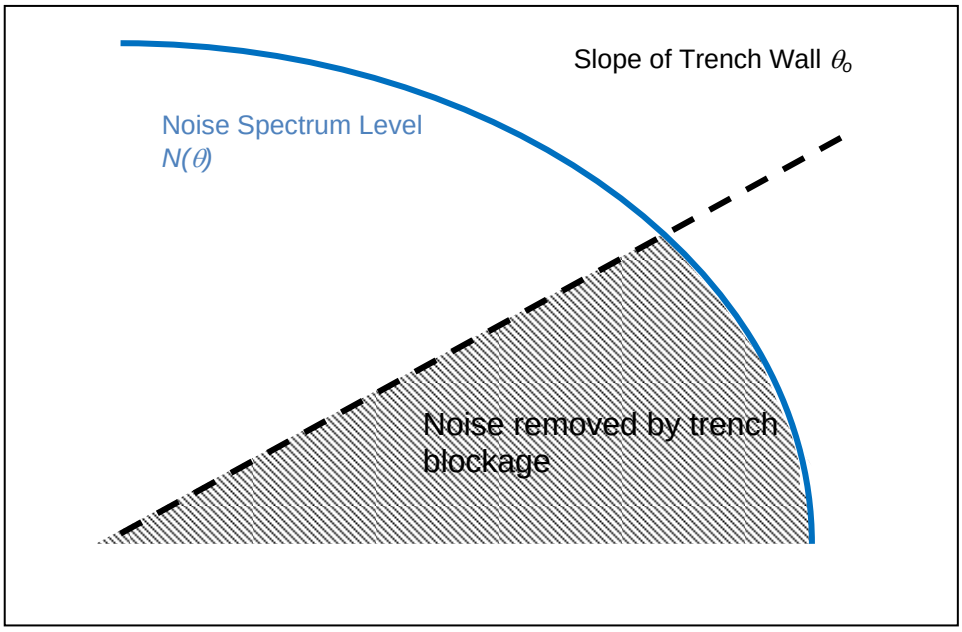

Figure 28. Graphical representation of the noise calculation showing the noise removed by the trench slope θ_o.

1. Azimuth Independent Calculation

The simplest assumption for calculating the noise levels in a trench is that the sensor is blocked on all sides by the bathymetry. This is similar to the sensor being placed in a hole in the ocean floor with θ_o constant at all azimuths ϕ. Calculating the noise area removed by this method simply involves treating the area calculated by Equation 3 as a solid of revolution to get the full noise volume.

$$N_{tot} = \int_0^{2\pi} \int_{\theta_o(\phi)}^{\frac{\pi}{2}} N(\theta) \cos\theta \, d\theta \, d\phi \tag{5}$$

where N_{tot} is the total noise volume reaching the sensor in the trench. The factor $\cos\theta$ accounts for the spherical nature of the receiver field and reduces the noise concentration per steradian as the elevation angle increases.

2. Azimuth Dependent Calculation

An alternate assumption is that the trench is a parallel trough on the ocean bottom and the area of noise intensity removed depends on the angle ϕ to the sensor. Therefore, $N(\theta)$ is modeled in segments of n intervals over a quadrant to account for the variations in noise volume.

$$N_{tot} = \frac{2\pi}{n} \sum_{\phi=\frac{\pi}{2n}}^{\frac{\pi}{2}} \int_{\theta_o(\phi)}^{\frac{\pi}{2}} N(\theta) \cos\theta d\theta \tag{6}$$

n=number of segments

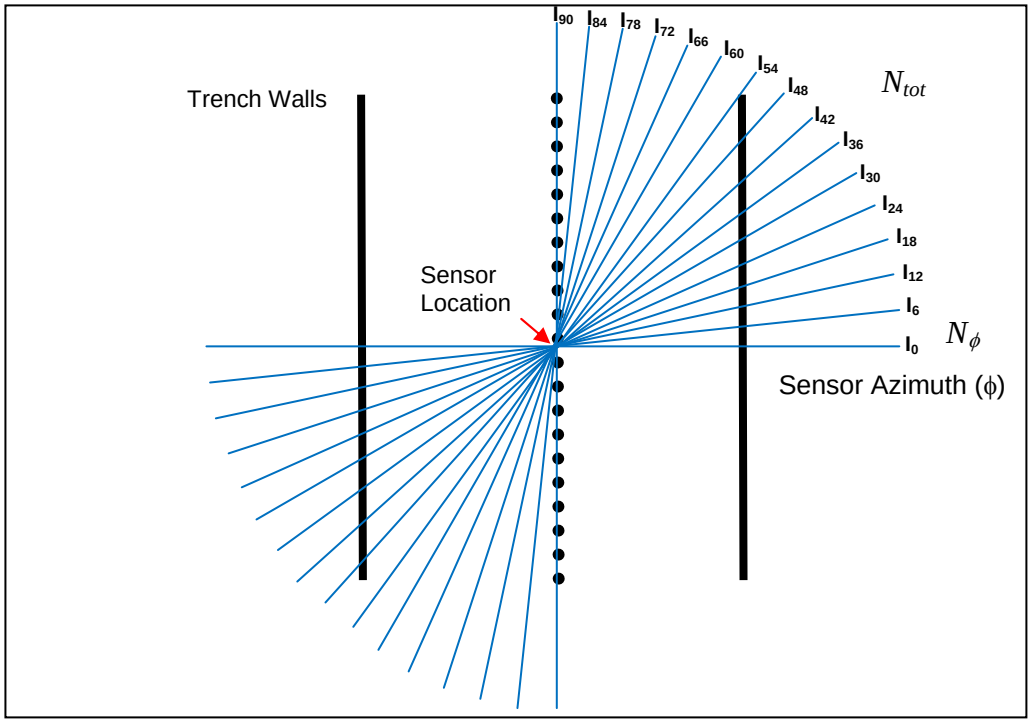

Figure 29. Overhead graphical representation showing the segments of N_ϕ at each azimuth ϕ which make up the total volume removed by the trench (N_{tot}).

The ratio difference between N_{tot} to the noise level without the trench bathymetry (N_{ref}) represents the decibel change (ΔdB) in noise caused by the trench, as shown in Equation 7.

$$\Delta dB = 10 \log \left(\frac{N_{tot}}{N_{ref}} \right) \tag{7}$$

3. Results

The azimuth-independent noise calculation for Trenches A and B shows a decrease in noise levels of 4.6 dB and 2.2 dB respectively. Since low-frequency noise arriving from horizontal ranges has 250 times greater intensity than overhead sources, low trench walls remove a significant amount of the total noise energy from the environment. Trench A reduces the noise level by 65% while Trench B removes 40% of the noise energy from the environment.

Using the azimuth-dependent calculation shows a decrease of 2.4 dB for Trench A and 1.4 dB for Trench B. Since the trench slope decreases at angles near $\phi = 90^{o}$ when using the azimuth dependent calculation, it is expected that the noise reduction will not be as great as with the azimuth independent model.

At higher frequencies (>300 Hz), where the maximum noise energy begins to arrive from steeper vertical angles, it is not expected that the trench will cause a significant decrease in noise energy.

4. Other Examples

Along with the representative trenches above, localized canyons and ridges around the subduction zones have the potential to provide steeper angles and improved SNR. Figure 30 shows how noise level changes with the angle from the sensor to the top of the trench, using the azimuth dependent calculation. A canyon with 30-degree walls can decrease noise by 7.5 dB and, at 45 degrees, the reduction is 10 dB. Ridges, where

there is only a single wall to block noise ($\theta_{lower\ wall} = 0^o$), the maximum decrease is limited to 3 dB, since only half of the noise field can be blocked.

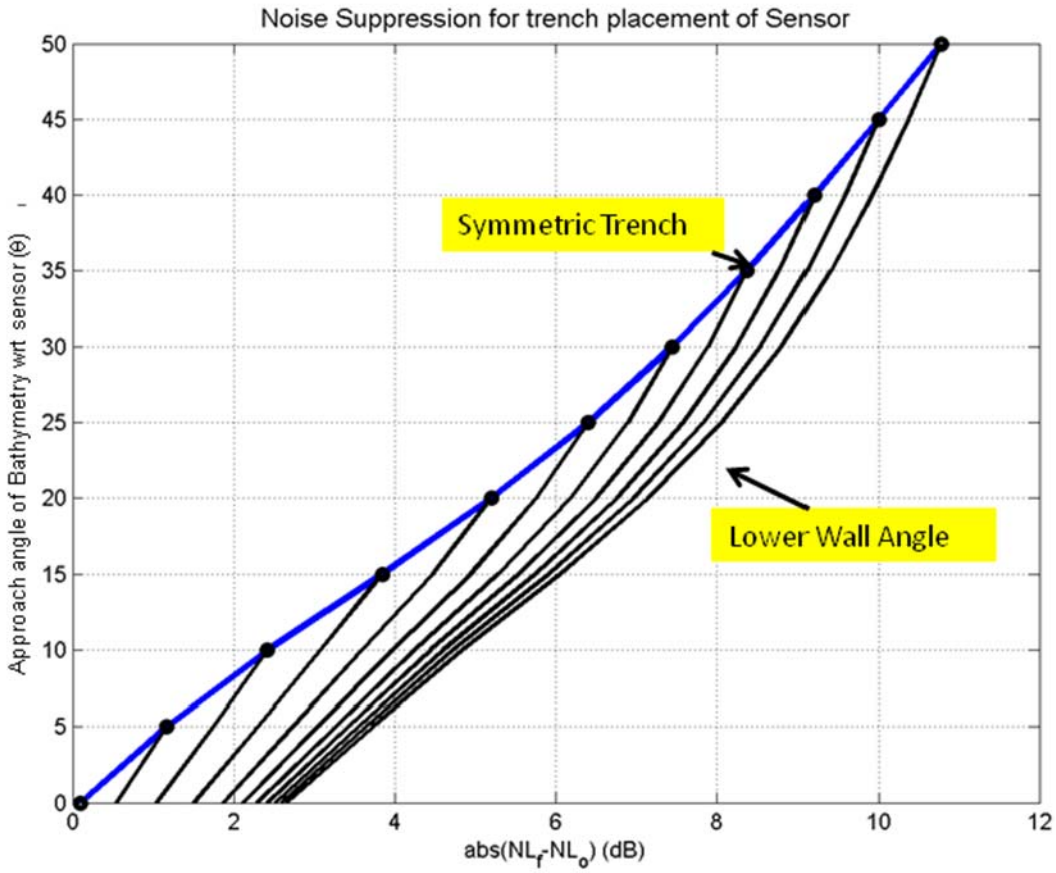

Figure 30. Noise suppression data for sensor placement within a trench for symmetric (blue) and uneven trenches based on the angle of the lower wall (black).

5. Factors Not Considered in Noise Calculations

The noise mechanisms in Trench B (subduction trench) are more complex than either calculation can fully account for due to its vast size and depth. Pressure is the main driver of sound speed below the DSC, and the SSP has a positive speed gradient that deflects sound upward. The noise calculation for both models assumes isospeed when calculating directional effects of noise propagation. However, upward deflecting sound is less likely to be blocked by low-slope bathymetry, meaning that the noise reduction calculation for Trench B is likely an overestimation.

The deep placement of sensors means sound emanating from near the surface needs to travel nearly vertical to reach the sensor due to sound speed deflection. As such, noise that emanates from distant sources travels on a path that undergoes several surface and bottom reflections before reaching the sensor. Figure 19 shows that signal level in Trench B drops significantly on the continental side of the trench. Shallow areas such as coastal water will subject traveling noise to greater attenuation than deeper ocean environments. Therefore, placing the sensor low in a trench can improve ambient noise levels through effects other than blockage.

Assuming a uniform noise environment, the high wall on Trench B can remove sound from half the field giving up to a 3dB possible reduction in noise. However, it is likely that the continental shelf will have higher ambient noise levels than the open ocean due to a greater presence of local traffic. Therefore, having a higher wall towards the continental shelf means the stronger contribution to the ambient noise is suppressed.

Calculations in Matlab, along with empirical data for the noise curves in Figure 27, are available in Appendices A–D.

THIS PAGE INTENTIONALLY LEFT BLANK

VI. SENSOR-TO-SENSOR COMMUNICATIONS

A. DEEP SOUND CHANNEL PROPAGATION

The high walls and ridge formations around trenches have the potential to create obstacles to modem-to-modem communications by physical obstruction within the DSC. This can result in reflection, attenuation, and scattering of the signal, reducing the strength and hindering communications.

The following simulations consider a 5000 m long seamount between a pair of modems obstructing their communication channel. The seamount is 10–15 km from the transmitting modem. The maximum depth of the seamount is varied to assess how the overall transmission capability is affected.

The optimal communications modem placement is at or just below the DSC axis. The gateway node can connect either to this DSC node or directly to a seabed node. The operating frequencies of the acoustic modems should be as low as practical, while still retaining adequate spectral bandwidth. The recommend Deep Seaweb communications band is below 8 kHz. Traditional Seaweb operating bands are closer to 12 kHz [14].

1. On-Axis Modem Results

The source is placed on the DSC axis at a depth of 1000 m, corresponding to the optimum location. Figure 32 shows the different-sized seamounts, and Figure 31 shows the effect each has on the communication signal. Obstructions below 1000 m do not impact the signal transmission significantly. This is mainly due to the fact that, at this depth, the signal can travel horizontally through the DSC channel with little variation in path. The interference that does exist comes from sporadic destructive interference of the signal as the reflected multipath converges with the non-reflected path. With the seamount at shallower depths above 1000 m, the effects become more apparent, and the obstructions result in shadow zones where no signal can reach the receiver. The effect becomes even greater when the seamount cuts through a larger cross-section of the channel. At 500 m, the channel is effectively blocked.

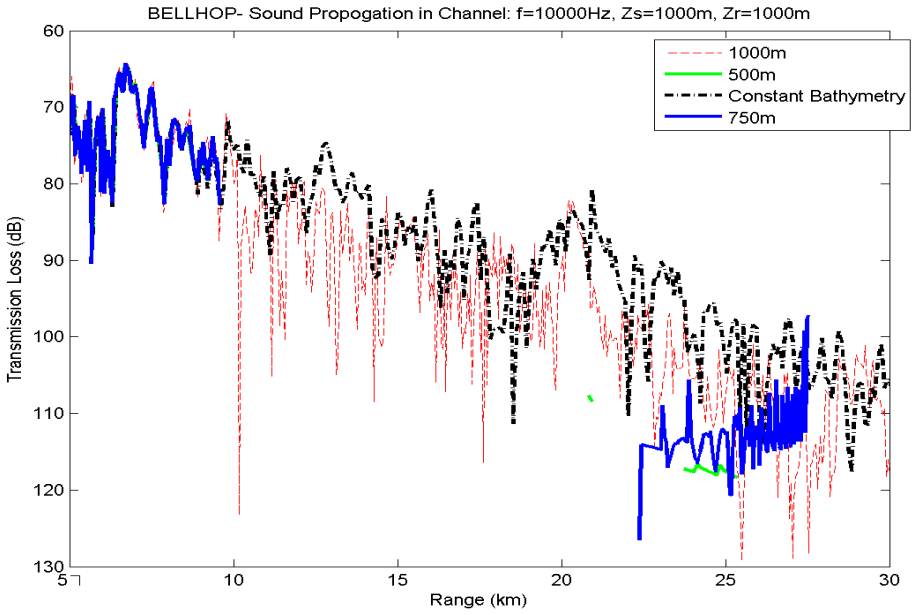

Figure 31. Modem 10 kHz TL vs. Range for obstructed DSC with on-axis modem.

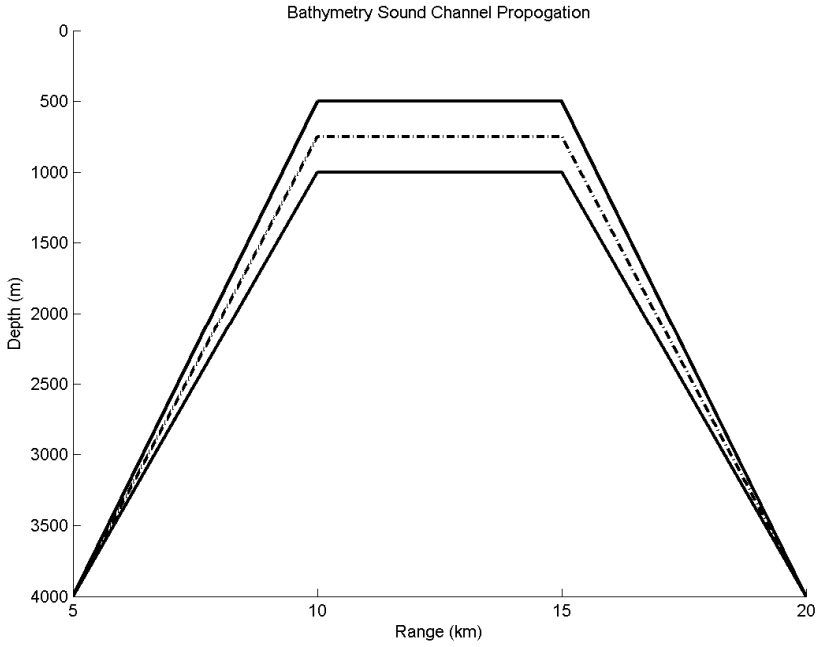

Figure 32. Bathymetry vs. Range for Figure 31.

2. Offset-Axis Modem Results

With the source on the DSC axis, the communication channel is theoretically optimized and will experience the least transmission loss. This placement is not likely in an operational environment due to currents that will cause the modem to shift away from the DSC axis. It is known, from prior testing, that placement off the axis results in a larger refracted path with increased propagation and greater attenuation [14]. Propagation is modeled for a source at 1200 m (offset 200 m below DSC axis) with seamount heights of 1500 m, 1000 m, and 750 m. Figure 33 shows the results of the off-axis simulation, which are similar to the on-axis modeling for signal blockage.

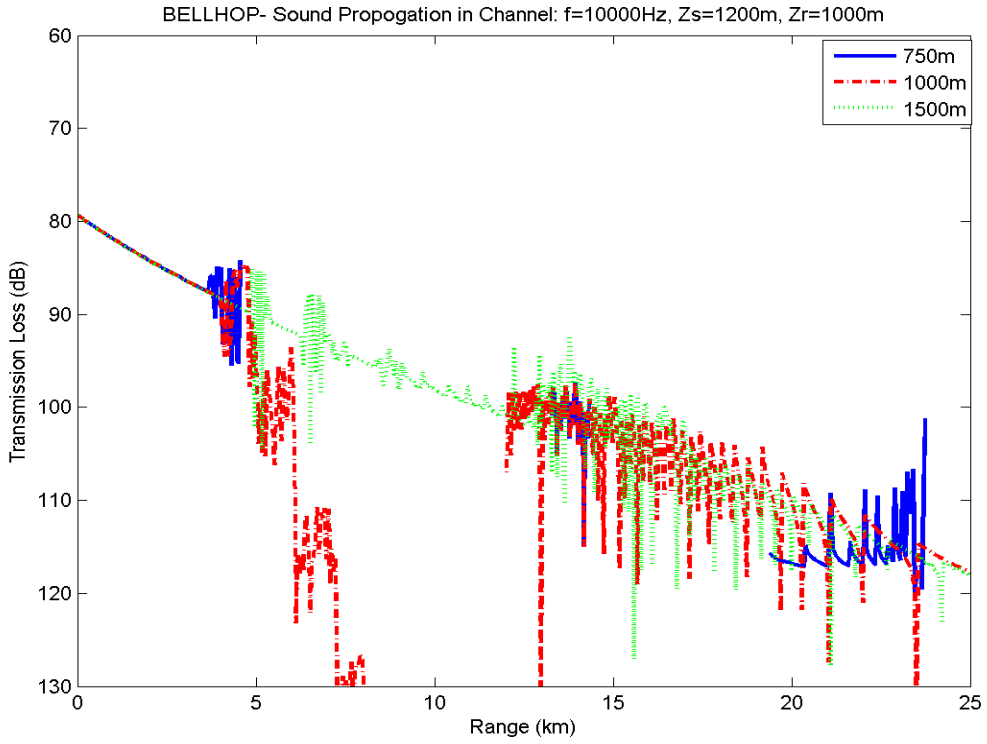

Figure 33. Modem 10 kHz TL vs. Range for obstructed DSC with off-axis modem.

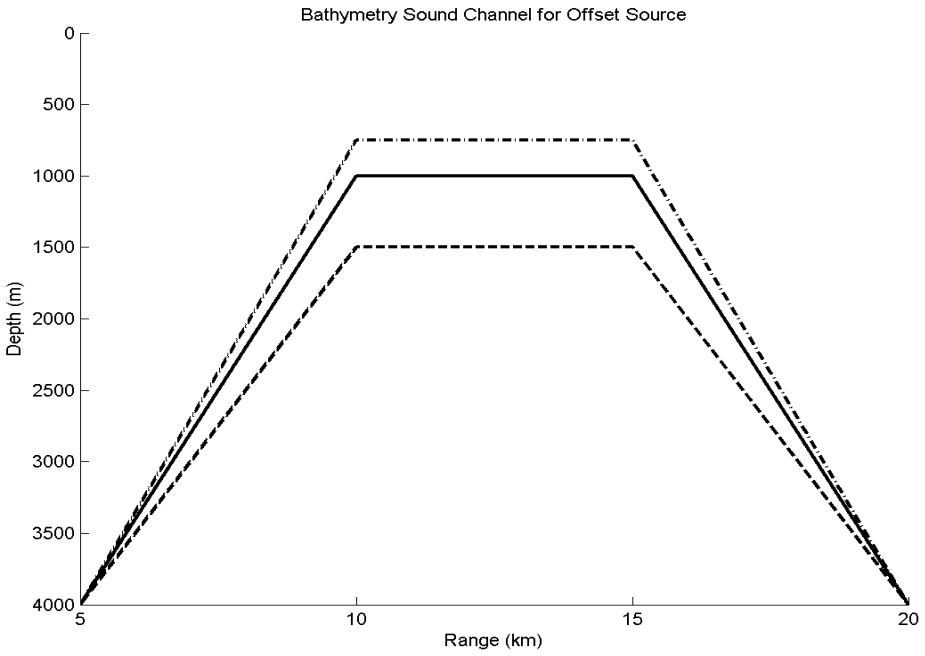

Figure 34. Bathymetry vs. Range for Figure 33.

VII. CONCLUSION, RECOMMENDATIONS, WAY AHEAD

Seaweb has been tested extensively in various stressful environments. The system has a high maturity level and the ability to detect contacts in areas with high levels of background noise. Deep Seaweb is a more recent concept that uses many of the advancements of Seaweb technology for application in the open ocean with greater coverage. Deep Seaweb exploits greater ocean depths and sound channel features for improved sensor performance and longer communication links.

Exploiting bathymetry can further improve Deep Seaweb's effectiveness. Simulation results show that placement of the sensors at the bottom of a deep ocean trench improves signal reception by concentrating and amplifying the acoustic signal from a vessel of interest. Moreover, trenches provide significantly reduced ambient noise levels by blocking horizontally arriving low-frequency noise resulting in improved SNR for better detection and fewer false alarms.

The dynamics and environmental characteristics of trenches are not well understood. Deep placement of the system should mitigate variations from temperature and pressure on the propagation of sound reaching the sensors. The noise models do not account for flow noise or seismic events possible within deep ocean trenches, which can increase the noise level at the sensor. In addition, variations in the bathymetry or the characteristics of the ocean floor can affect the performance of the sensor in ways not expected. More complex trench models to simulate sound and noise propagation are necessary to better understand environmental impact on the system.

Development and testing of Deep Seaweb in an operational environment is the next step towards deployment of the system as an autonomous acoustic network that can support enforcement of maritime law and interdiction of illegal activities in open waters.

THIS PAGE INTENTIONALLY LEFT BLANK

LIST OF REFERENCES

[1] A Cooperative Strategy for 21st Century Seapower, October 2007.

[2] The National Strategy for Maritime Security, September 2005.

[3] United Nations Convention on the Law of the Sea, 10 December 1982

[4] Office of Naval Research, Division 321. Text. http://www.onr.navy.mil/Science-Technology/Departments/Code-32/All-Programs/Ocean-Systems-321/Undersea-Signal-Processing.aspx (accessed 29 May 2010).

[5] Naval Operations Concept 2010 (NOC10), Implementing the Maritime Strategy, May 2010.

[6] Plate Tectonics. Text. http://www.platetectonics.com/book/page_12.asp (accessed 20 May 2010).

[7] Geo-engineering Extreme Events Reconnaissance (GEER) Association. Image. www.geerassociation.org/.../seismological.html (accessed 20 May 2010).

[8] Wikipedia; Ocean Trench. Text. http://en.wikipedia.org/wiki/Oceanic_trench (accessed 20 May 2010).

[9] United States Geological Survey's (USGS) Earthquake Hazards Program. Image. http://earthquake.usgs.gov/earthquakes/world/puerto_rico/puerto_rico_trench.php (accessed 20 May 2010).

[10] Wikimedia; Plate Tectonic Boundaries Map created by Eric Gaba. Image. http://upload.wikimedia.org/wikipedia/commons/thumb/b/bf/Tectonic_plates_boundaries_detailed-en.svg/2000px-Tectonic_plates_boundaries_detailed-en.svg.png (accessed 23 May 2010).

[11] J. A. Rice, "Seaweb Acoustic Communication and Navigation Networks," *Proc. Conf. Underwater Acoustic Measurements: Technologies & Results*, Heraklion, Greece (2005).

[12] J. Rice, Deep Seaweb presentation, unpublished (2008).

[13] G. M. Wenz, "Acoustic Ambient Noise in the Ocean: Spectra and Sources," *The Journal of the Acoustical Society of America*, vol. 34, no. 12, pp. 1936–1956, December 1962.

[14] S. R. Thompson, "Sound Propagation Considerations for a Deep-Ocean Acoustic Network," M.S. thesis, Naval Postgraduate School, Monterey, CA, 2009.

[15] F. B. Jensen, W. A. Kuperman, M. B. Porter, and H. Schmidt. *Computational Ocean Acoustics*. New York: Springer-Verlag New York, Inc., 2000.

[16] W. H. Munk, *Sound Channel in an exponentially stratified ocean, with application to SOFAR,* Institute of Geophysics and Planetary Physics, Scripps Institution of Oceanography, 1974.

[17] A. L. Maggi and A. J. Duncan, "AcTUP v2.2i^{α} Acoustic Toolbox Installation and User Guide," Curtin University of Technology, Centre for Marine Science and Technology. Available: http://cmst.curtin.edu.au/local/docs/products/actup_v2_2l_installation_user_guide.pdf (accessed 2 June 2010).

[18] O. C. Rodriguez, "General description of the bellhop ray tracing program - version 1.0," Universidade do Algarve – Physics Department, Tech. Rep., June 2008. Available: http://oalib.hlsresearch.com/Rays/GeneralDescription.pdf (accessed 28 May 2010).

[19] E. H. Axelrod, B. A. Schoomer and W. A. Von Winkle, "Vertical Directionality of Ambient Noise in the Deep Ocean at a Site near Bermuda," *The Journal of the Acoustical Society of America*, vol. 37, no. 1, pp. 77–83, January 1965.

APPENDIX A. AZIMUTH INDEPENDENT NOISE MODEL MATLAB CODE

```
%This program calculates the change in noise intensity in
%Trenches A&B using azimuth independence and a -40dB
%base for angles blocked by the trench walls

 clear all
  load NoiseCurve

%% Define trench parameters
 L1=13000;    %Trench 1 length (m)
 D1=2330;     %Trench 1 depth (m)
 L21=48000;   %Trench 2 side1 length (m)
 L22=65000;   %Trench 2 side2 length (m)
 D21=3350;    %Trench 2 side 1 depth (m)
 D22=8850;    %Trench 2 side2 depth (m)

%% Calculate noise from graph

% file 'NoiseCurve' contains measurements for x and y of the noise curve.  Those
% values are referenced to values of dB
 db0=1.06;     %reference length for dB=0
 db30=2.12;    %reference length for dB=30

 ddb=30/(db30-db0);

 x=(noisecurve(:,1));
 y=(noisecurve(:,2));

 noisecurve112(:,1) = (0:.001:max(noisecurve(:,1)));
 noisecurve112(:,2)=interp1(x,y,noisecurve112(:,1));

 noisecurve112(:,3)=ddb.*noisecurve112(:,1);
 noisecurve112(:,4)=ddb.*noisecurve112(:,2);

% calculate angle phi of points on noise curve
 phi=atan(noisecurve112(:,2)./noisecurve112(:,1));

 %calculate noise intensity
 noisecurve112(:,5)=10.^(noisecurve112(:,3)./10);
 noisecurve112(:,6)=10.^(noisecurve112(:,4)./10);
```

```
 figure (1); plot (noisecurve112(:,3),noisecurve112(:,4));
 title ('Reference Noise Level (dB)')

 figure (2); plot (noisecurve112(:,5),noisecurve112(:,6));
 title ('Reference Noise Level Intensity')

%% Defining -40Db power
 db40=0.0001.*(max(noisecurve112(:,5)));  %noise level 40dB below max noise level
 I40=0.5*pi*(db40)^2;                     %40dB area of a half disc

%% reference noise
 Iref=pi.*max(noisecurve112(:,5)).*trapz(noisecurve112(:,5),noisecurve112(:,6));

%% Intergrating Noise Level Trench A
 n2=0;
 Itot=0;
 phi_t=atan(D1/L1);
 m=1;

 while (phi(m,1)>phi_t)
   m=m+1;
 end

 phi_r=phi(m,1);
 I=pi.*noisecurve112(m,5).*(trapz(noisecurve112(1:m,5),noisecurve112(1:m,6))-
trapz(noisecurve112(1:m,5),(noisecurve112(m,6)./noisecurve112(m,5)).*noisecurve112(
1:m,5)));
 Itot=Itot+I;

%Total change in noise level in dB
 dBchange=10*log10(Itot/Iref);
 disp(['Noise Level decrease for Trench A =' ,num2str(abs(dBchange)), 'dB']);

%% Integrating Noise Level Trench B

%side 1
 n2=0;
 Itot21=0;
 phi_t=atan(D21/L21);
 m=1;

 while (phi(m,1)>phi_t)
   m=m+1;
 end
```

```
 phi_r=phi(m,1);
 I=pi.*noisecurve112(m,5).*(trapz(noisecurve112(1:m,5),noisecurve112(1:m,6))-
trapz(noisecurve112(1:m,5),(noisecurve112(m,6)./noisecurve112(m,5)).*noisecurve112(
1:m,5)));+I40*phi_r/pi;
 Itot21=Itot21+I;

%side 2
 n2=0;
 Itot22=0;
 phi_t=atan(D22/L22);
 m=1;

 while (phi(m,1)>phi_t)
   m=m+1;
 end

 phi_r=phi(m,1);
 I=pi.*noisecurve112(m,5).*(trapz(noisecurve112(1:m,5),noisecurve112(1:m,6))-
trapz(noisecurve112(1:m,5),(noisecurve112(m,6)./noisecurve112(m,5)).*noisecurve112(
1:m,5)))+I40*phi_r/pi;
 Itot22=Itot22+I;

%Total change in noise level in dB
 dBchange=10*log10((Itot21+Itot22)/(2*Iref));
 disp(['Noise Level decrease for Trench B =' ,num2str(abs(dBchange)), 'dB']);
```

THIS PAGE INTENTIONALLY LEFT BLANK

APPENDIX B. AZIMUTH DEPENDENT NOISE MODEL MATLAB CODE

```
%This program calculates the change in noise intensity in
%Trenches A&B using azimuth dependence and a -40dB
%base for angles blocked by the trench walls

 clear all
 load NoiseCurve

%% Define trench parameters
 L1=13000;    %Trench 1 length (m)
 D1=2330;     %Trench 1 depth (m)
 L21=48000;   %Trench 2 side1 length (m)
 L22=65000;   %Trench 2 side2 length (m)
 D21=3350;    %Trench 2 side 1 depth (m)
 D22=8850;    %Trench 2 side2 depth (m)

%% Calculate noise from graph

% file 'NoiseCurve' contains measurements for x and y of the noise curve.  Those
% values are referenced to values of dB/str
 db0=1.06;     %reference length for dB=0
 db30=2.12;    %reference length for dB=30

 ddb=30/(db30-db0);

 x=(noisecurve(:,1));
 y=(noisecurve(:,2));

 noisecurve112(:,1) = (0:.001:max(noisecurve(:,1)));
 noisecurve112(:,2)=interp1(x,y,noisecurve112(:,1));

 noisecurve112(:,3)=ddb.*noisecurve112(:,1);
 noisecurve112(:,4)=ddb.*noisecurve112(:,2);

% calculate angle theta of points on noise curve
 phi=atan(noisecurve112(:,2)./noisecurve112(:,1));

%calculate noise intensity
 noisecurve112(:,5)=10.^(noisecurve112(:,3)./10);
 noisecurve112(:,6)=10.^(noisecurve112(:,4)./10);
```

```
 figure (1); plot (noisecurve112(:,3),noisecurve112(:,4));
 title ('Reference Noise Level (dB)')

 figure (2); plot (noisecurve112(:,5),noisecurve112(:,6));
 title ('Reference Noise Level Intensity')


%% Defining -40dB power
 db40=0.0001.*(max(noisecurve112(:,5)));  %noise level 40dB below max noise level
 I40=0.5*pi*(db40)^2;                     %40dB area of a half disc

%reference noise
 Iref=pi.*max(noisecurve112(:,5)).*trapz(noisecurve112(:,5),noisecurve112(:,6));

%% Integrating Noise Level Trench A
 n2=0;
 Itot=0;

 for n=pi/180:pi/180:pi/2
    n2=n2+1;
    L=L1/cos(n);
    phi_t=atan(D1/L);
    m=1;

    while (phi(m,1)>phi_t)
        m=m+1;
    end

    phi_r=phi(m,1);
    I=(pi.*noisecurve112(m,5).*(trapz(noisecurve112(1:m,5),noisecurve112(1:m,6))-
trapz(noisecurve112(1:m,5),(noisecurve112(m,6)./noisecurve112(m,5)).*noisecurve112
(1:m,5))))+I40*phi_r/pi;

    Itot=Itot+I;
 end

%Calculating total noise power
 Itot=Itot/n2;

%Total change in noise level in dB
 dBchange=10*log10(Itot/Iref);
 disp(['Noise Level change for Trench A =' ,num2str(abs(dBchange)), 'dB']);

%% Integrating Noise Level Trench B

%side 1
```

```
 n2=0;
 Itot1=0;

 for n=pi/180:pi/180:pi/2
   n2=n2+1;
   L=L21/cos(n);
   phi_t=atan(D21/L);
   m=1;

   while (phi(m,1)>phi_t)
      m=m+1;
   end

   phi_r=phi(m,1);

   I=(pi.*noisecurve112(m,5).*(trapz(noisecurve112(1:m,5),noisecurve112(1:m,6))-
trapz(noisecurve112(1:m,5),(noisecurve112(m,6)./noisecurve112(m,5)).*noisecurve112
(1:m,5))))+I40*phi_r/pi;

   Itot1=Itot1+I;
 end

%Calculating total noise power
 Itot1=Itot1/n2;

%side 2
 n2=0;
 Itot2=0;

 for n=pi/180:pi/180:pi/2
   n2=n2+1;
   L=L22/cos(n);
   phi_t=atan(D22/L);
   m=1;

   while (phi(m,1)>phi_t)
      m=m+1;
   end

   phi_r=phi(m,1);
   I=(pi.*noisecurve112(m,5).*(trapz(noisecurve112(1:m,5),noisecurve112(1:m,6))-
trapz(noisecurve112(1:m,5),(noisecurve112(m,6)./noisecurve112(m,5)).*noisecurve112
(1:m,5))))+I40*phi_r/pi;
```

```
    Itot2=Itot2+I;
  end

%Calculating total noise power
  Itot2=Itot2/n2;
  Itot=(Itot1+Itot2)/2;

%Total change in noise level in dB
  dBchange=10*log10(Itot/Iref);
  disp(['Noise Level change for Trench B =' ,num2str(abs(dBchange)), 'dB']);
```

APPENDIX C. NOISE SUPPRESION GRAPH MATLAB CODE

```
%This program calculates the change in noise energy level in
%trenches over a range of angles and creates a graph of the numbers
%using a -40dB base for angles blocked by the trench walls

 clear all
 load NoiseCurve

%% Calculate noise from graph

% file 'NoiseCurve' contains measurements for x and y of the noise curve.  Those
% values are referenced to values of dB
 db0=1.06;      %reference length for dB=0
 db30=2.12;    %reference length for dB=30

 ddb=30/(db30-db0);

 x=(noisecurve(:,1));
 y=(noisecurve(:,2));

 noisecurve112(:,1) = (0:.001:max(noisecurve(:,1)));
 noisecurve112(:,2)=interp1(x,y,noisecurve112(:,1));

 noisecurve112(:,3)=ddb.*noisecurve112(:,1);
 noisecurve112(:,4)=ddb.*noisecurve112(:,2);

% calculate angle phi of points on noise curve
 phi=atan(noisecurve112(:,2)./noisecurve112(:,1));

%calculate noise intensity
 noisecurve112(:,5)=10.^(noisecurve112(:,3)./10);
 noisecurve112(:,6)=10.^(noisecurve112(:,4)./10);

%% Defining -40Db power
 db40=0.0001.*(max(noisecurve112(:,5)));  %noise level 40dB below max noise level
 I40=0.5*pi*(db40)^2;    %40dB area of a half disc

%% Integrating Noise Level Trench A

%reference noise
 Iref=pi.*max(noisecurve112(:,5)).*trapz(noisecurve112(:,5),noisecurve112(:,6));
 k=0;
```

```
 for phi_i=0:pi/36:10*pi/36
   k=k+1;
   n=0;
   Itot=0;

   for theta=pi/1800:pi/1800:pi/2
      n=n+1;
      phi_t=atan(tan(phi_i)*cos(theta));
      m=1;

      while (phi(m,1)>phi_t)
        m=m+1;
      end

      phi_r=phi(m,1);
      I=(pi.*noisecurve112(m,5).*(trapz(noisecurve112(1:m,5),noisecurve112(1:m,6))-
trapz(noisecurve112(1:m,5),(noisecurve112(m,6)./noisecurve112(m,5)).*noisecurve112
(1:m,5))))+I40*phi_r/pi;
      Itot=Itot+I;
   end

%Calculating total noise intensity
   Itot=Itot/n;
   Itot_t(k,1)=Itot;
   Itot_t(1,1)=Iref;

%% Build Table for Values of DB vs. Phi
   dBchange(k,1)=phi_i*180/pi;       %phi values
   dBchange(k,2)=abs(10*log10(Itot/Iref));  %dB values
   j=1;

   while j<=k
      Itot_t(j,k)=(Itot_t(k,1)+Itot_t(j,1))/2;
      dBchange(j,k+2)=abs(10*log10(Itot_t(j,k)/Iref));
      j=j+1;
   end

 end

%% Build Plot
 figure (3); plot(dBchange(:,2),dBchange(:,1),'-bo','LineWidth',3,...
 'MarkerEdgeColor','k','MarkerSize',5);
 title('Noise Suppression for Trench Placement of Sensor','fontsize',12);
```

```
xlabel('abs(NL_f-NL_o) (dB)','fontsize',10);
ylabel('Approach angle of bathymetry wrt sensor (\phi)','fontsize',10);

hold all

for d=1:1:k
  plot (dBchange(1:d,d+2),dBchange(1:d,1),'-k','linewidth',2);
end
grid on;
```

THIS PAGE INTENTIONALLY LEFT BLANK

APPENDIX D. NOISECURVE DATA

Calculations for noise levels using code in Appendix A-C is based on the 112Hz graph in Figure 27 for Beaufort <4 wind levels. The following table is a representation of this graph in x-y coordinates and loaded in file **Noisecurve.m** utilized by those codes.

x	y	x (db)	y (db)
1.95	0	55.18867925	0
1.94	0.05	54.90566038	1.41509434
1.91	0.1	54.05660377	2.830188679
1.9	0.15	53.77358491	4.245283019
1.88	0.2	53.20754717	5.660377358
1.86	0.25	52.64150943	7.075471698
1.83	0.3	51.79245283	8.490566038
1.8	0.35	50.94339623	9.905660377
1.76	0.41	49.81132075	11.60377358
1.72	0.46	48.67924528	13.01886792
1.68	0.51	47.54716981	14.43396226
1.63	0.57	46.13207547	16.13207547
1.58	0.63	44.71698113	17.83018868
1.54	0.67	43.58490566	18.96226415
1.48	0.71	41.88679245	20.09433962
1.43	0.75	40.47169811	21.22641509
1.39	0.79	39.33962264	22.35849057
1.32	0.83	37.35849057	23.49056604
1.26	0.86	35.66037736	24.33962264
1.21	0.89	34.24528302	25.18867925
1.15	0.92	32.54716981	26.03773585
1.08	0.94	30.56603774	26.60377358
1.01	0.97	28.58490566	27.45283019
0.94	1	26.60377358	28.30188679
0.86	1.02	24.33962264	28.86792453
0.77	1.05	21.79245283	29.71698113
0.68	1.07	19.24528302	30.28301887
0.61	1.08	17.26415094	30.56603774
0.51	1.09	14.43396226	30.8490566
0.45	1.095	12.73584906	30.99056604
0.38	1.095	10.75471698	30.99056604
0.33	1.1	9.339622642	31.13207547
0.28	1.1	7.924528302	31.13207547
0.23	1.1	6.509433962	31.13207547
0.18	1.1	5.094339623	31.13207547
0.13	1.1	3.679245283	31.13207547
0.08	1.1	2.264150943	31.13207547
0.03	1.1	0.849056604	31.13207547
0	1.1	0	31.13207547

THIS PAGE INTENTIONALLY LEFT BLANK

INITIAL DISTRIBUTION LIST

1. Defense Technical Information Center
   Ft. Belvoir, Virginia

2. Dudley Knox Library
   Naval Postgraduate School
   Monterey, California

3. Professor Joseph Rice
   Naval Postgraduate School
   Monterey, California

4. Professor Kevin Smith
   Naval Postgraduate School
   Monterey, California

5. Professor Daphne Kapolka
   Naval Postgraduate School
   Monterey, California

6. Professor Andres Larraza
   Naval Postgraduate School
   Monterey, California

7. RADM Richard (Rick) Williams (Ret.), USN
   Naval Postgraduate School
   Monterey, California

8. James Ehlert
   Naval Postgraduate School
   Monterey, California

9. RADM Gerald Ellis (Ret.), USN
   Naval Postgraduate School
   Monterey, California

10. CDR Jonathan Vanslyke, USN
    Naval Postgraduate School
    Monterey, California

11. CDR Daniel Chisholm, USN
Naval Postgraduate School
Monterey, California

12. Gary Wilson
ARLUT
Austin, Texas

13. Martin Barlett
ARLUT
Austin, Texas

14. LT Pongaskorn Sommai, Royal Thai Navy
Naval Postgraduate School
Monterey, California

15. Eryn Wezensky
Naval Postgraduate School
Monterey, California

16. ME5 Meng Chong Goh, Royal Singapore Navy
Naval Postgraduate School
Monterey, California

17. ENS William Jenkins, USN
Naval Postgraduate School
Monterey, California

18. Robert Creber
SSC Pacific
San Diego, California

19. Christopher Fletcher
SSC Pacific
San Diego, California

20. Dale Green
Teledyne Benthos, Inc.
North Falmouth, Massachusetts

21. Fred Scali
JIATF-S
Key West, Florida

22. Brian Tipton
MIT/LL
Lexington, Massachusetts

23. Fred Waugh
MIT/LL
Lexington, Massachusetts